Arabian Journal of Chemistry (2022) **15**, 104291

King Saud University

Arabian Journal of Chemistry

www.ksu.edu.sa
www.sciencedirect.com

ORIGINAL ARTICLE

Chicken and duck eggshell beads modified with iron (III) oxide-hydroxide and zinc oxide for reactive blue 4 dye removal

Pornsawai Praipipat [a,b,*], **Pimploy Ngamsurach** [a,b], **Chonthicha Saekrathok** [a], **Sukanya Phomtai** [a]

[a] *Department of Environmental Science, Khon Kaen University, Khon Kaen 40002, Thailand*
[b] *Environmental Applications of Recycled and Natural Materials (EARN) Laboratory, Khon Kaen University, Khon Kaen 40002, Thailand*

Received 28 June 2022; accepted 18 September 2022
Available online 26 September 2022

KEYWORDS

Food waste;
Metal oxide;
Anionic dye;
Adsorption;
Wastewater treatment

Abstract Releasing contaminated dyes into water bodies might create environmental problems for water quality and toxic aquatic organisms. The toxicity of dyes might affect human health throughout the food chain, so it is necessary to treat contaminated dye in wastewater before discharging it into the water body. Chicken eggshell beads (CB), duck eggshell beads (DB), chicken eggshell beads mixed iron (III) oxide-hydroxide (CBF), duck eggshell beads mixed iron (III) oxide-hydroxide (DBF), chicken eggshell beads mixed zinc oxide (CBZ), and duck eggshell beads mixed zinc oxide (DBZ) were synthesized, and several characterized techniques of XRD, FESEM-FIB, EDX, and FTIR were used to identify the crystalline structure, surface morphology, and chemical composition and functional groups. Reactive blue 4 (RB4) dye removal efficiencies on dye adsorbent materials were investigated through batch experiments with varying doses, contact time, temperature, pH, and concentration. Their adsorption patterns and mechanisms also were studied by adsorption isotherm and kinetics. All dye adsorbent materials demonstrated semi-crystalline structures, and their surface morphologies had a spherical shape with coarse surfaces. Oxygen, carbon, calcium, chlorine, and sodium and four main function groups of O—H, N—H, C—O, and C—O—C were detected in all dye adsorbent materials. For batch tests, they could remove RB4 dye by more than 56%, and CBF represented the highest RB4 dye removal efficiency at 84.44%. Moreover, the addition of iron (III) oxide-hydroxide and zinc oxide helped to improve RB4 dye adsorbent efficiencies which an

* Corresponding author.
E-mail addresses: pornprai@kku.ac.th (P. Praipipat), pimploy@kkumail.com (P. Ngamsurach), s_chonthicha@kkumail.com (C. Saekrathok), sukanya.prom@kkumail.com (S. Phomtai).
Peer review under responsibility of King Saud University.

Production and hosting by Elsevier

https://doi.org/10.1016/j.arabjc.2022.104291

iron (III) oxide-hydroxide increased RB4 removal efficiency of chicken and duck eggshell beads more than zinc oxide. Their adsorption patterns and mechanisms were well explained by Freundlich and pseudo-second-order kinetic models. Therefore, all dye adsorbent materials especially CBF are potential dye adsorbent materials for further industrial applications.

1. Introduction

Many industries are used dyes in their manufacturing processes of pigments, paint, and textile, they might discharge contaminated dye into water bodies. These create environmental concerns of sunlight blocking of aquatic plants and algae, and they are toxic to aquatic organisms (Lellis et al., 2019). In addition, the utilization of contaminated water and consumption of aquatic animals might result in human health effects of allergy, dermatitis, skin irritation, and skin cancer (Manzoor and Sharma, 2019). Among various types of dye, reactive dyes are popularly used for dyeing cellulose fibers because of their long-lasting color; however, it is difficult for natural bio-degradation because of a stable polyaromatic molecule (Chavan, 2011). Therefore, the treatment of contaminated dyes in wastewater is required before discharging to receiving waters for a safe environment.

Although many methods are normally used for dye removals in aqueous solutions such as chemical precipitation, coagulation-flocculation, advanced oxidation process, photocatalytic degradation, reverse osmosis, ion-exchange, and adsorption (Katheresan et al., 2018), the adsorption is an effective method with easy operation and reasonable cost (Omo-Okoro et al., 2018). However, a key of high adsorption is a good pick of adsorbent with saving operating cost, so many studies have been developed on low-cost adsorbents from agriculture, industrial, food wastes such as sawdust, rice husk, bagasse fly ash, bagasse, coconut shells, shrimp shells, banana peels, and eggshells for dye removals in wastewater. In previous studies, rice husk and coconut shell have been used for removing reactive blue 4, maxilon blue GRL, and direct yellow 12 in an aqueous solution (Aljeboree et al., 2017; Chowdhury and Saha, 2016), and sawdust was also used to eliminate reactive blue 4 (Teixeira et al., 2021). Moreover, the potato peel, pumpkin seed, and eggshell could be used for removing reactive blue 49, cibacrom blue P3R, reactive black 5, and basic fuchsin in wastewater (Bouhadjra et al., 2021; Çelebi, 2019). Among those, chicken and duck eggshells are interesting choices because not only they have good chemical properties of calcium carbonate ($CaCO_3$) for dye removals (Bessashia et al., 2020) but also they help to reduce a hug of food waste as recycled waste for wastewater treatment as well.

Many studies have applied several metal oxides to improve dye removal efficiencies of adsorbent materials such as copper oxide (CuO), aluminum oxide (Al_2O_3), manganese oxide (MnO), titanium dioxide (TiO_2), iron oxide (FeOH), zinc oxide (ZnO) (Nayeri and Mousavi, 2020). The modification of titanium (IV) oxide and calcium alginate was used for basic blue 41 removal, and the nanomaterial of Zn-Al-Fe_3O_4 sodium alginate beads has also used for rhodamin B removal in an aqueous solution (M. Kumar et al., 2019; Nouri et al., 2020). Especially, iron (III) oxide-hydroxide and ZnO are popularly used for improving material efficiencies to remove dyes in many articles (Ngamsurach et al., 2022). Many previous studies used zinc oxide to modify various nanomaterials and hybrid beads for removing various dye colors such as methylene blue, basic blue 41, acid black 210, reactive blue 19, eriochrome black T, crystal violet, and brilliant green (Elsayed et al., 2022; Kaur et al., 2021; Kumar et al., 2018; Monsef Khoshhesab and Souhani, 2018; Shokry Hassan et al., 2014). In addition, Fe_3O_4 was widely used for modifying sugarcane bagasse and alginate beads to eliminate methylene blue, malachite green, reactive red 535, remazol brilliant blue R, congo red, and direct red 23 (Buthiyappan et al., 2019; Lv and Li, 2021). Therefore, this study attempts to synthesize dye adsorbent materials by adding metal oxides of iron (III) oxide-hydroxide and zinc oxide to improve dye material efficiencies from chicken and duck eggshell beads for dye removals in an aqueous solution for further industrial applications.

This current research attempted to synthesize six dye adsorbent materials of chicken eggshell beads (CB), duck eggshell beads (DB), chicken eggshell beads mixed iron (III) oxide-hydroxide (CBF), duck eggshell beads mixed iron (III) oxide-hydroxide (DBF), chicken eggshell beads mixed zinc oxide (CBZ), and duck eggshell beads mixed zinc oxide (DBZ) for removals of reactive blue 4 dye (RB4) in an aqueous solution, to identify their characterizations with several techniques of X-ray Diffractometer (XRD), Field Emission Scanning Electron Microscopy and Focus Ion Beam (FESEM-FIB), Energy Dispersive X-ray Spectrometer (EDX), Fourier Transform Infrared Spectroscopy (FTIR), and Thermogravimetric Analysis and Differential Thermal Gravimetry (TGA/DTG) to investigate their RB4 dye removal efficiencies with affecting factors of dosage, contact time, temperature, pH, and initial concentration by a series of batch experiments, and to study their adsorption isotherm, kinetics, and thermodynamic.

2. Materials and methods

2.1. Raw materials

Chicken and duck eggshells were collected from the local restaurants in Khon Kaen province, Thailand.

2.2. Raw material preparations

Chicken and duck eggshells were washed with tap water to eliminate contaminations, and then they were dried overnight in a hot air oven (Binder, FED 53, Germany) at 80 °C. Then, they were ground and sieved in size of 125 μm, and they were kept in a desiccator before use called chicken eggshell powder (CP) and duck eggshell powder (DP).

2.3. Chemicals

All chemicals were analytical grades (AR) without purification before use. Ferric chloride hexahydrate ($FeCl_3{\cdot}6H_2O$) (LOBA, India), sodium hydroxide (NaOH) (RCI Labscan, Thailand), and zinc oxide (ZnO) (QRëC, New Zealand) were used for modified bead materials. Sodium alginate ($NaC_6H_7O_6$) (Merck, Germany) and calcium chloride ($CaCl_2$) (Kemaus, New Zealand) were used for the bead formation. Reactive blue 4 (RB4) ($C_{23}H_{14}Cl_2N_6O_8S_2$) (Sigma-Aldrich, Germany) whose chemical structure is shown in Fig. 1 was used for preparing of synthetic dye solution. 0.1 M Hydrochloric acid (HCl) (RCI Labscan, Thailand) and 0.1 M sodium chloride (NaCl) (RCI Labscan, Thailand) were used for the point of zero charge. Finally, 0.5 % of 65 % nitric acid (HNO_3) (Merck, Germany) and 0.5 % NaOH (RCI Labscan, Thailand) were used for pH adjustments.

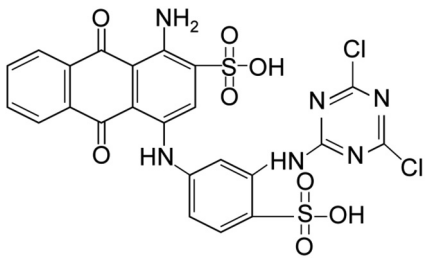

Fig. 1 The chemical structure of RB4.

2.4. The preparation of dye solution

The stock solution of reactive blue 4 (RB4) of 100 mg/L concentration was prepared by adding 0.1 g RB4 into a 100 mL beaker containing 50 mL deionized water (DI), then it was mixed with a glass rod and poured into 1000 mL volumetric flask. Next, approximately 950 mL of DI water was added to obtain the volume of 1000 mL.

2.5. Material synthesis

Fig. 2 demonstrated the synthesis of all dye adsorbent materials, and the details were clearly explained below:

2.5.1. The synthesis of chicken and duck eggshell beads (CB or DB)

Firstly, 10 g of CP or DP were added to 400 mL of 2 % sodium alginate and were heated by a hot plate (Ingenieurbüro CAT, M. Zipperer GmbH, M 6, Germany) at 60 °C with a stable stirring speed of 200 rpm. Next, the samples were added dropwise into 250 mL of 0.1 M $CaCl_2$ by using a syringe with a needle (1.2 mm × 40 mm) and soaked in 0.1 M $CaCl_2$ solution for 24 h. Then, they were filtrated, rinsed with DI water, and air-dried at room temperature for 12 h. Finally, the samples were kept in desiccators before use called chicken eggshell beads (CB) or duck eggshell beads (DB).

2.5.2. The synthesis of chicken and duck eggshell beads mixed iron (III) oxide-hydroxide (CBF or DBF)

Firstly, 10 g of CP or DP were added to 160 mL of 5 % $FeCl_3 \cdot 6H_2O$, and they were mixed by an orbital shaker (GFL, 3020, Germany) of 200 rpm for 3 h. Then, the samples were filtrated and air-dried at room temperature for 12 h. Next, the samples were added to 160 mL of 5 % NaOH and they were shaken by an orbital shaker of 200 rpm for 1 h. After that, they were filtered and air-dried at room temperature for 12 h and kept in desiccators before use called chicken eggshell powder mixed iron (III) oxide-hydroxide (CPF) or duck eggshell powder mixed iron (III) oxide-hydroxide (DPF). Next, CPF or DPF were added to 400 mL of 2 % sodium alginate, and then they were homogeneously mixed and heated by a hot plate at 60 °C with a constant stirring of 200 rpm. Then, the samples were added dropwise into 250 mL of 0.1 M $CaCl_2$ by using a 10 mL syringe with a needle size of 1.2 × 40 mm. The beaded samples were soaked in 0.1 M $CaCl_2$ for 24 h, and then they were filtered and rinsed with DI water. After that, they were air-dried at room temperature for 12 h and kept in desiccators before use called chicken eggshell beads mixed iron (III) oxide-hydroxide (CBF) or duck eggshell beads mixed iron (III) oxide-hydroxide (DBF).

2.5.3. The synthesis of chicken or duck eggshell beads mixed zinc oxide (CBZ or DBZ)

Firstly, 10 g of CP or DP were added to 160 mL of 5 % zinc oxide, and they were mixed by an orbital shaker of 200 rpm for 3 h. Then, the samples were filtered and air-dried at 12 h, and they were kept in a desiccator called chicken eggshell powder mixed zinc oxide (CPZ) or duck eggshell powder mixed zinc oxide (DPZ). Next, CPZ or DPZ were added to 400 mL of 2 % sodium alginate, and then they were homogeneously mixed and heated by a hot plate at 60 °C with a constant stirring of 200 rpm. Then, the samples were added dropwise into 250 mL of 0.1 M $CaCl_2$ by using a 10 mL syringe with a needle size of 1.2 × 40 mm. The beaded samples were soaked in 0.1 M $CaCl_2$ for 24 h, and then they were filtered and rinsed with DI water. After that, they were air-dried at room temperature for 12 h and kept in desiccators before use called chicken eggshell beads mixed zinc oxide (CBZ) or duck eggshell beads mixed zinc oxide (DBZ).

2.6. Characterization of dye adsorbent materials

Five analytical techniques were used to determine the crystalline structures, surface morphologies, chemical compositions, chemical functional groups, and mass changes as temperature changes of all dye adsorbent materials. For crystalline structures, X-ray Diffractometer (XRD) (Bruker, D8 Advance, Switzerland) in a range of 2θ = 5-80° was used. For surface morphologies and chemical compositions, Field Emission Scanning Electron Microscopy and Focus Ion Beam (FESEM-FIB) with Energy Dispersive X-ray Spectrometer (EDX) (FEI, Helios NanoLab G3 CX, USA) were applied. For chemical functional groups, Fourier Transform Infrared Spectroscopy (FTIR) (Bruker, TENSOR27, Hong Kong) in a range of 4000–600 cm^{-1} was used. For the measurement of mass changes in dye adsorbent materials as a function of temperature, Thermogravimetric Analysis and Differential Thermal Gravimetry (TGA/DTG) (Rigaku, ThermoPlus TG8120, Japan) were used at a temperature range of 30–800 °C at a heating rate of 10 °C per minute in N_2 atmosphere.

2.7. The point of zero charge of dye adsorbent materials for RB4 dye removal

The sample solutions of 0.1 M NaCl with adjusting pH from 2 to 12 by 0.1 M HCl and 0.1 M NaOH were used for studying the point of zero charge of dye adsorbent materials for RB4 dye removal. For each sample solution, 0.1 g of each dye adsorbent material was added to 250 mL Erlenmeyer flasks containing 50 mL of 0.1 M NaCl. Next, it was shaken by an orbital shaker (GFL, 3020, Germany) at room temperature at 150 rpm for 24 h. Then, a final pH value of the sample solution was measured by a pH meter (Mettler Toledo, SevenGo with InLab 413/IP67, Switzerland) and calculated ΔpH (pH_{final} – $pH_{initial}$). The value of the point of zero charge (pH_{pzc}) is a point which is the crosses line of ΔpH versus $pH_{initial}$ equal to zero.

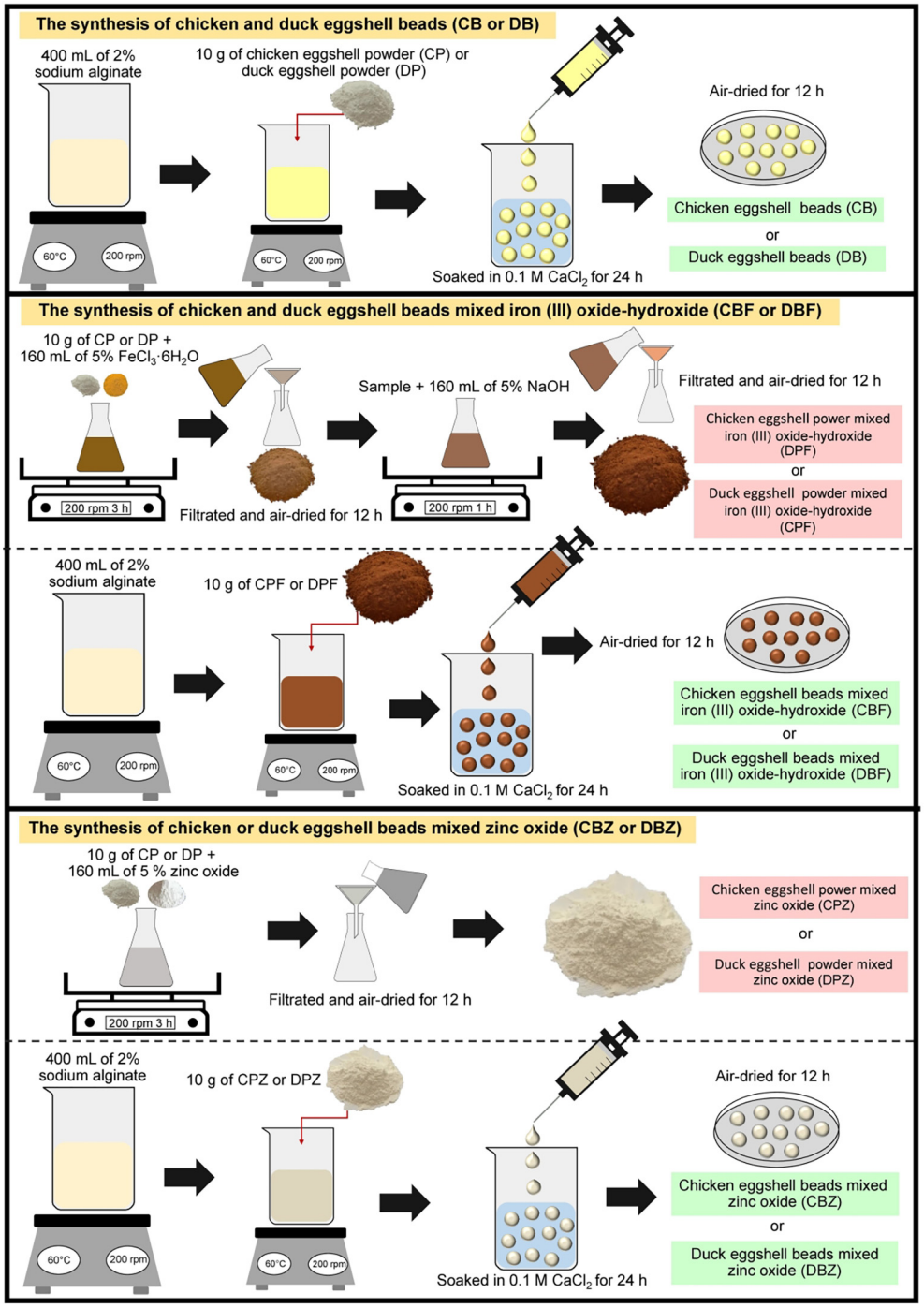

Fig. 2 The synthesis of chicken eggshell beads (CB), duck eggshell beads (DB), chicken eggshell beads mixed iron (III) oxide-hydroxide (CBF), duck eggshell beads mixed iron (III) oxide hydroxide (DBF), chicken eggshell beads mixed zinc oxide (CBZ), and duck eggshell beads mixed zinc oxide (DBZ).

2.8. Batch experiments

Batch experiments were designed to demonstrate RB4 dye removal efficiencies of dye adsorbent materials with varying doses, contact time, temperature, pH, and concentration. UV–vis Spectrophotometer (Hitachi, UH5300, Japan) was used to analyze dye concentrations of all samples, and the details of batch experiments were explained below:

2.8.1. Effect of dose

Six different dosages from 0.1 to 0.6 g were used for investigating RB4 dye removal efficiencies on all dye adsorbent materials with the control condition of a sample volume of 100 mL, the RB4 dye concentration of 50 mg/L, a shaking speed of 150 rpm, a contact time for 12 h, the temperature of 50 °C, and pH 7. The optimum dose was chosen from the lowest material dose with the highest RB4 dye removal efficiency,

and it was used in the next experiment on the contact time effect.

2.8.2. Effect of contact time

Six different contact times from 3 to 18 h were used for investigating RB4 dye removal efficiencies on all dye adsorbent materials with the control condition of a sample volume of 100 mL, the RB4 dye concentration of 50 mg/L, a shaking speed of 150 rpm, the temperature of 50 °C, pH 7, and the optimum dose. The optimum contact time was chosen from the lowest contact time with the highest RB4 dye removal efficiency, and it was used in the next experiment on temperature effect.

2.8.3. Effect of temperature

Six different temperatures from 30 to 80 °C were used for investigating RB4 dye removal efficiencies on all dye adsorbent materials with the control condition of a sample volume of 100 mL, the RB4 dye concentration of 50 mg/L, a shaking speed of 150 rpm, pH 7, and the optimum dose and contact time. The optimum temperature was chosen from the lowest temperature with the highest RB4 dye removal efficiency, and it was used for the next experiment on the pH effect.

2.8.4. Effect of pH

pH values of 3, 5, 7, 9, and 11 were used for investigating RB4 dye removal efficiencies on all dye adsorbent materials with the control condition of a sample volume of 100 mL, the RB4 dye concentration of 50 mg/L, a shaking speed of 150 rpm, pH 7, and the optimum dose, contact time, and temperature. The optimum pH was chosen from the pH value obtained the highest RB4 dye removal efficiency, and it was used in the next experiment on concentration effect.

2.8.5. Effect of concentration

Seven different concentrations from 30 to 90 mg/L were used for investigating RB4 dye removal efficiencies on all dye adsorbent materials with the control condition of a sample volume of 100 mL, the RB4 dye concentration of 50 mg/L, a shaking speed of 150 rpm, and the optimum dose, contact time, temperature, and pH. The optimum RB4 dye concentration was chosen from the highest RB4 dye removal efficiency.

Triplicate experiments were conducted to confirm the results, and the average values were reported. Eq. (1) was used to calculate dye removal efficiency in the percentage.

$$\text{Dye removal efficiency } (\%) = \left(\frac{C_0 - C_e}{C_0}\right) \times 100 \tag{1}$$

where C_e is the equilibrium of dye concentration (mg/L), and C_0 is the initial dye concentration (mg/L).

2.9. Adsorption isotherms

Adsorption isotherms were used to descript the adsorption patterns of RB4 adsorbed on dye adsorbent materials by using both linear and nonlinear Langmuir, Freundlich, Temkin, and Dubinin-Radushkevich isotherms following Eqs. (2)-(9) (Dubinin and Radushkevich, 1947; Freundlich, 1906; Langmuir, 1918; Temkin and Pyzhev, 1940):

Langmuir isotherm:

$$\text{Linear}: \frac{C_e}{q_e} = \frac{1}{q_m K_L} + \frac{C_e}{q_m} \tag{2}$$

$$\text{Nonlinear}: q_e = \frac{q_m K_L C_e}{1 + K_L C_e} \tag{3}$$

Freundlich isotherm:

$$\text{Linear}: \log q_e = \log K_F + \frac{1}{n} \log C_e \tag{4}$$

$$\text{Nonlinear}: q_e = K_F C_e^{1/n} \tag{5}$$

Temkin isotherm:

$$\text{Linear}: q_e = \frac{RT}{b_T} \ln A_T + \frac{RT}{b_T} \ln C_e \tag{6}$$

$$\text{Nonlinear}: q_e = \frac{RT}{b_T} \ln A_T C_e \tag{7}$$

Dubinin-Radushkevich:

$$\text{Linear}: \ln q_e = \ln q_m - K_{DR} \varepsilon^2 \tag{8}$$

$$\text{Nonlinear}: q_e = q_m \exp(-K_{DR} \varepsilon^2) \tag{9}$$

where q_e is the capacity of dye adsorption on dye adsorbent materials at equilibrium (mg/g), q_m is the maximum amount of dye adsorption on dye adsorbent materials (mg/g), C_e is the equilibrium of dye concentration (mg/L), K_L is Langmuir adsorption constant (L/mg), K_F is Freundlich constant of adsorption capacity (mg/g)(L/mg)$^{1/n}$, and n is the constant depicting of the adsorption intensity (Jangkorn et al., 2022). R is the universal gas constant (8.314 J/mol K), T is the absolute temperature (K), b_T is the constant related to the heat of adsorption (J/mol), and A_T is the equilibrium binding constant corresponding to maximum binding energy (L/g). q_m is the theoretical saturation adsorption capacity (mg/g), K_{DR} is the activity coefficient related to mean adsorption energy (mol^2/J^2), and ε is the Polanyi potential (J/mol) (Threepanich and Praipipat, 2021). Graphs of linear Langmuir, Freundlich, Temkin, and Dubinin-Radushkevich isotherms were plotted by C_e/q_e versus C_e, log q_e versus log C_e, q_e versus ln C_e, and ln q_e versus ε^2, respectively whereas graphs of their nonlinear were plotted by q_e versus C_e.

For the adsorption isotherm experiment, the optimum dose of dye adsorbent materials was applied with various RB4 dye concentrations from 30 to 90 mg/L with the control condition of a sample volume of 100 mL, a contact time 12 h, the temperature of 50 °C, pH 7, and a shaking speed of 150 rpm.

2.10. Adsorption kinetics

The adsorption rate and mechanism of dye adsorbent materials were explained by studying adsorption kinetics in both linear and nonlinear pseudo-first-order, pseudo-second-order, elovich, and intra-particle diffusion models following Eqs. (10)-(16) (Elovich and Larinov, 1962; Ho and McKay, 1999; Lagergren, 1898; Weber and Morris, 1963):

Pseudo-first-order kinetic model:

$$\text{Linear}: \ln(q_e - q_t) = \ln q_e - k_1 t \tag{10}$$

$$\text{Nonlinear}: q_t = q_e\left(1 - e^{-k_1 t}\right) \quad (11)$$

Pseudo-second-order kinetic model:

$$\text{Linear}: \frac{t}{q_t} = \frac{1}{k_2 q_e^2} + \left(\frac{1}{q_e}\right)t \quad (12)$$

$$\text{Nonlinear}: q_t = \frac{k_2 q_e^2 t}{1 + q_e k_2 t} \quad (13)$$

Elovich model:

$$\text{Linear}: q_t = \frac{1}{\beta}\ln(\alpha\beta) + \frac{1}{\beta}\ln t \quad (14)$$

$$\text{Nonlinear}: q_t = \beta \ln t + \beta \ln \alpha \quad (15)$$

Intra-particle diffusion model:

$$\text{Linear and nonlinear}: q_t = k_i t^{0.5} + C_i \quad (16)$$

where q_e (mg/g) and q_t (mg/g) are the capacities of dye adsorbed by dye adsorbent materials at equilibrium and at the time (t), respectively. k_1 (min^{-1}), k_2 (g/mg•min), k_i (mg/g•$min^{0.5}$) are the reaction of rate constants of pseudo-first-order, pseudo-second-order, and intra-particle diffusion models, respectively (Jangkorn et al., 2022). α is the initial adsorption rate (mg/g/min) and β is the extent of surface coverage (g/mg). C_i is the constant that gives an idea about the thickness of the boundary layer (mg/g) (Threepanich and Praipipat, 2021). Graphs of linear pseudo-first-order, pseudo-second-order, elovich, and intra-particle diffusion models were plotted by $\ln(q_e - q_t)$ versus time (t), t/q_t versus time (t), q_t versus $\ln t$, and q_t versus time ($t^{0.5}$), respectively whereas their nonlinear graphs were plotted by the capacity of dye adsorbed by dye adsorbent materials at the time (q_t) versus time (t).

For the adsorption kinetic experiment, the optimum dose of dye adsorbent materials was applied with the control condition of RB4 dye concentration of 50 mg/L, a sample volume of 1000 mL, a contact time of 15 h, the temperature of 50 °C, pH 7, and a shaking speed of 150 rpm.

2.11. Thermodynamic study

Thermodynamic studies were the investigation of temperature effect in a range of 303–353 K on the adsorption capacities of all dye adsorption materials for RB4 dye removal which three thermodynamic parameters of Gibb free energy ($\Delta G°$), standard enthalpy change ($\Delta H°$), and standard entropy change ($\Delta S°$) were applied to explain the results. Their parameters were calculated following Eq. (17) - (19) (Kumar et al., 2018).

$$\Delta G^O = -RT\ln K_L \quad (17)$$

$$\ln K_L = -\frac{\Delta H^O}{RT} + \frac{\Delta S^O}{R} \quad (18)$$

$$\Delta G^O = \Delta H^o - T\Delta S^o \quad (19)$$

where R is the universal gas constant (8.314 J/mol K), T is the absolute temperature (K), and K_L is the Langmuir constant (L/mg). A graph of $\ln K_0$ ($K_0 = q_e/C_e$) and $1/T$ is plotted to determine the values of $\Delta H°$ and $\Delta S°$ from the slope and intercept of its linear (Bessashia et al., 2020). For $\Delta G°$ is calculated from Eq. (17).

For the thermodynamic experiment, the optimum dose of dye adsorbent materials was applied with various temperatures of 30-80 °C or 303–353 K with the control condition of RB4 dye concentration of 50 mg/L, a sample volume of 100 mL, a contact time 12 h, pH 7, and a shaking speed of 150 rpm.

3. Results and discussion

3.1. The physical characteristic of dye adsorbent materials

The physical characteristics of dye adsorbent materials were demonstrated in Fig. 3a–3f which had a spherical shape with different colors depending on raw materials and types of metal oxide inside materials. For CB and DB, CB was a cream-beaded color whereas DB was a light-cream-beaded color and chicken eggshells had a darker cream color than duck eggshells shown in Fig. 3a and 3d. For CBF and DBF, both dye adsorbent materials had an iron-rust beaded color matched to the color of iron (III) oxide-hydroxide shown in Fig. 3b and 3e. For CBZ and DBZ, both dye adsorbent materials had a similar color to CB and DB which were a cream-beaded color and a light-cream-beaded color, respectively shown in Fig. 3c and 3f. Since zinc oxide is white color powder, it might not affect to change the color of dye adsorbent materials.

3.2. Characterizations of dye adsorbent materials

3.2.1. XRD

Crystalline structures of dye adsorbent materials by XRD analysis were demonstrated in Fig. 4a-4f which displayed the semi-crystalline structures. For CB and DB, they demonstrated semi-crystalline structures shown in Fig. 4a and 4b with specific calcium carbonate peaks of 29.54°, 30.86°, 36.08°, 39.52°, 43.36°, 47.66°, 48.76°, and 57.54° for CB and 23.10°, 29.46°, 36.02°, 39.40°, 43.24°, 47.54°, 48.58°, and 57.46° for DB matched to JCPDS No. 05–0586 (Hamdi and Habubi, 2018). In addition, they also found sodium alginate peaks of 13.26°, 18.56°, 20.32°, 21.76°, 24.24°, 28.10°, and 38.12° at low intensity (Lakouraj et al., 2014). For CBF and DBF, not only they detected the specified peaks similarly to CB and DB but also they displayed the specified iron (III) oxide-hydroxide peaks of 21.20°, 33.22°, 36.56°, 41.63°, and 53.74° relating to JCPDS No. 29–0713 (Huang et al., 2018) at low intensity shown in Fig. 4c and 4d. For CBZ and DBZ, they had specified peaks similarly to CB and DB, and they also had specified zinc oxide peaks of 31.92°, 34.64°, 36.48°, 47.68°, 56.74°, 62.98°, 68.20°, and 69.24° matching to JCPDS No. 36–1451 (Anbuvannan et al., 2015) at high intensity shown in Fig. 4e and 4f. As a result, they could be confirmed by the successfully adding of iron (III) oxide-hydroxide and zinc oxide into CP and DP to synthesize CBF, DBF, CBZ, and DBZ.

3.2.2. FESEM-FIB and EDX

The surface morphologies of dye adsorbent materials at 100X magnification with 1 mm in bead form and 2500X magnification with 50 μm in the surface by FESEM-FIB analysis were demonstrated in Fig. 5a-5l. For CB and DB, they had a spherical shape with coarse surfaces at 100X magnification with 1 mm shown in Fig. 5a and 5c, and their surface displayed coarse surfaces at 2500X magnification with 50 μm shown in Fig. 5b and 5d. For CBF and DBF, they had a spherical shape

Fig. 3 Physical characteristics of (a) chicken eggshell beads (CB), (b) chicken eggshell beads mixed iron (III) oxide-hydroxide (CBF), (c) chicken eggshell beads mixed zinc oxide (CBZ), (d) duck eggshell beads (DB), (e) duck eggshell beads mixed iron (III) oxide-hydroxide (DBF), and (f) duck eggshell beads mixed zinc oxide (DBZ).

with heterogenous and coarse surfaces similarly to CB and DB at 100X magnification with 1 mm shown in Fig. 5e and 5g, and their surfaces were also coarse surfaces at 2500X magnification with 50 μm shown in Fig. 5f and 5h. For CBZ and DBZ, their surfaces were similar to CBF and DBF in both 100X magnification with 1 mm and 2500X magnification with 50 μm shown in Fig. 5i–5l. As a result, it was no obvious difference in the surface morphologies of all dye adsorbent materials by FESEM-FIB analysis.

The chemical compositions of dye adsorbent materials by EDX analysis were demonstrated in Table 1, and five main elements of oxygen (O), carbon (C), calcium (Ca), chlorine (Cl), and sodium (Na) whereas iron (Fe) and zinc (Zn) were found only in dye materials modified with iron (III) oxide-hydroxide and zinc oxide. For CB and CBF, O, Ca, Cl, and Na were decreased whereas C and Fe were increased after adding iron (III) oxide-hydroxide. As a result, it could verify the successfully adding of Fe into chicken eggshell powder (CP) before setting of bead materials. For CB and CBZ, O, Ca, and Cl were decreased whereas C, Na, and Zn were increased after adding zinc oxide to confirm the addition of zinc oxide into chicken eggshell powder (CP) before setting of bead materials. For DB and DBF, O, C, Na, and Fe were increased whereas Ca and Cl were decreased after adding iron (III) oxide-hydroxide. As a result, it could verify the addition of Fe into duck eggshell powder (DP) before setting bead materials similarly to DBF. For DB and DBZ, O, Ca, and Cl were decreased whereas C, Na, and Zn were increased after adding zinc oxide into duck eggshell powder (DP) before setting bead materials similarly to DBZ. Therefore, raw materials and types of metal oxide are the main factors to affect chemical elements into dye adsorbent materials.

3.2.3. FTIR

The chemical functional groups of dye adsorbent materials by FTIR analysis were illustrated in Fig. 6a–6f which had four main function groups of O—H, N—H, C—O, and C—O—C. O—H represented the stretching of alcohol and acidic hydrogen group, and N—H demonstrated amines and amides in the protein fiber of eggshells (Tizo et al., 2018). C—O illustrated the starching of calcium carbonate (Lulit et al., 2019), and C—O—C presented the starching of sodium alginate (Lakouraj et al., 2014). Moreover, the details of functional groups with indicating positions by the wavelength of dye adsorbent materials are reported in Table 2.

3.2.4. TGA

The thermogravimetric analysis (TGA) and differential thermal gravimetry (DTG) performed at a temperature range of 30-800 °C at a heating rate of 10 °C per minute in N_2 atmosphere were used to determine the effect of temperature on dye adsorbent materials, and the results of TGA/DTG analysis are demonstrated in Fig. 7a–7f. For TGA analysis, the weight loss of all dye adsorbent materials is detected in five temperature ranges of 100-200 °C, 200-250 °C, 250-350 °C, 350-550 °C, and 550-800 °C, and their details are illustrated in Table 3. For a temperature range of 100-200 °C, the weight loss was due to the vaporization of dye adsorbent materials. In temperature ranges of 200-250 °C and 250-350 °C, they began the degradation of organic functional groups of chicken or duck eggshells in all dye adsorbent materials. The significant decomposition of the sample was found in a temperature range around 350-550 °C because of the conversion of calcium carbonate ($CaCO_3$) to calcium oxide (CaO) and carbon dioxide (CO_2), and its thermal decomposition ended approximately in a temperature range of 550-800 °C (Awogbemi et al., 2020). In five temperature ranges, CFB found a higher weight loss than CBZ and CB whereas the weight loss of DB had a higher effect than DBF and DBZ. Therefore, the temperature was an important factor resulting in the weight loss change of all dye adsorbent materials. For DTG analysis, the moisture contents in the dye

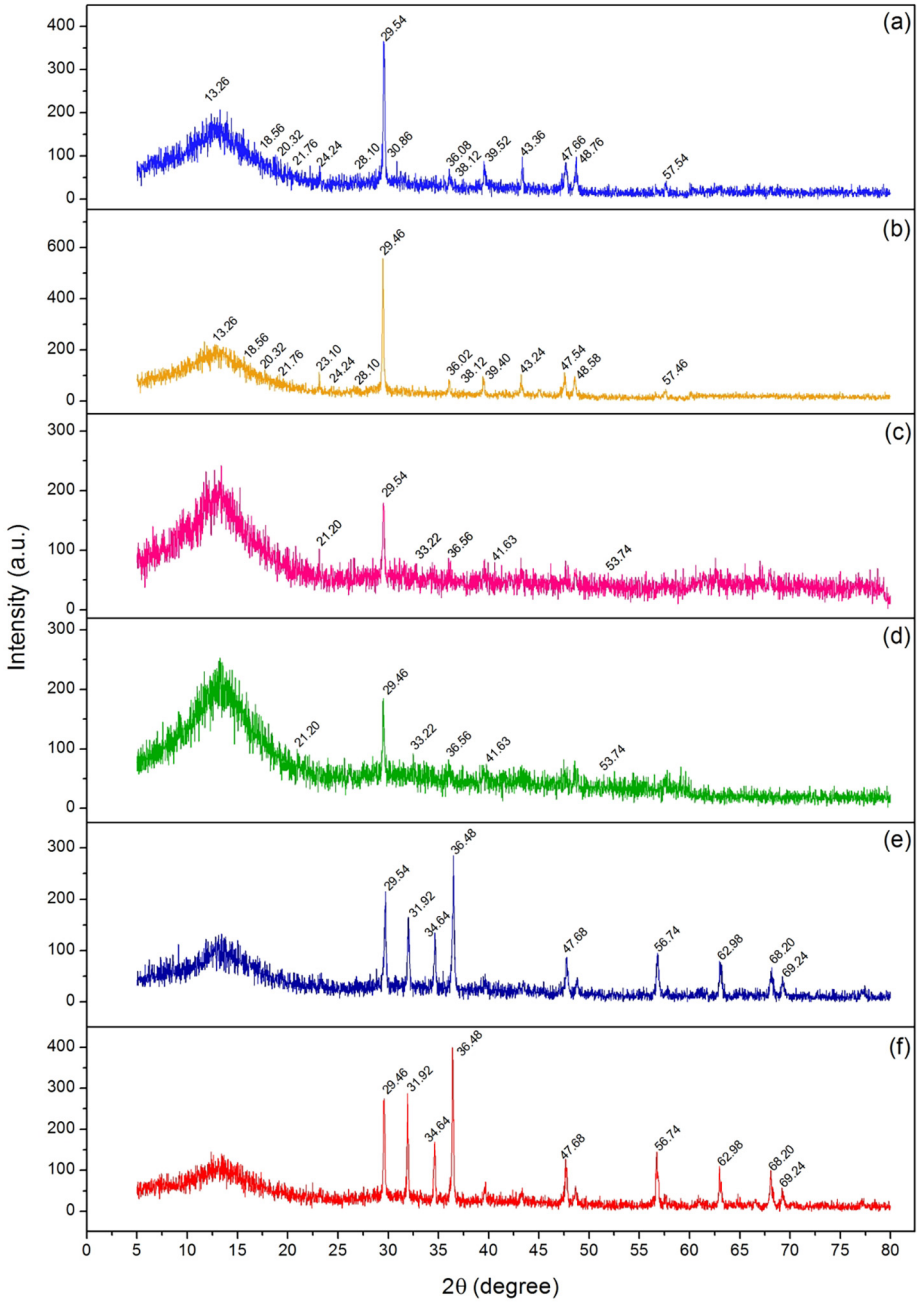

Fig. 4 Crystalline structures of (a) chicken eggshell beads (CB), (b) duck eggshell beads (DB), (c) chicken eggshell beads mixed iron (III) oxide-hydroxide (CBF), (d) duck eggshell beads mixed iron (III) oxide-hydroxide (DBF), (e) chicken eggshell beads mixed zinc oxide (CBZ), and (f) duck eggshell beads mixed zinc oxide (DBZ).

adsorbent materials were removed by detecting the endothermic peak around 100-200 °C. For other temperature ranges, they represented the exothermic peaks that corresponded to the decomposition of all dye adsorbent materials (Kumar et al., 2018).

3.3. The point of zero charge of dye adsorbent materials for RB4 dye removal

The studying of the point of zero charge of dye adsorbent materials for RB4 dye removal was designed to determine which pH value is good for RB4 dye adsorption by each dye adsorbent material. In principle, the point of zero charge (pH_{pzc}) means a pH value at the net charge equal to zero of the adsorbent (Rey et al., 2017). Fig. 8a and 8b are demonstrated pH_{pzc} of all dye adsorbent materials. The pH_{pzc} values of CB, CBF, and CBZ were 7.26, 7.56, and 7.44, respectively shown in Fig. 8a whereas the pH_{pzc} values of DB, DBF, and DBZ were 7.15, 7.47, and 7.30, respectively shown in Fig. 8b. As a result, the addition of iron (III) oxide-hydroxide and zinc oxide resulted in the increase of pH_{pzc} with a higher effect of an iron (III) oxide-hydroxide than zinc oxide.

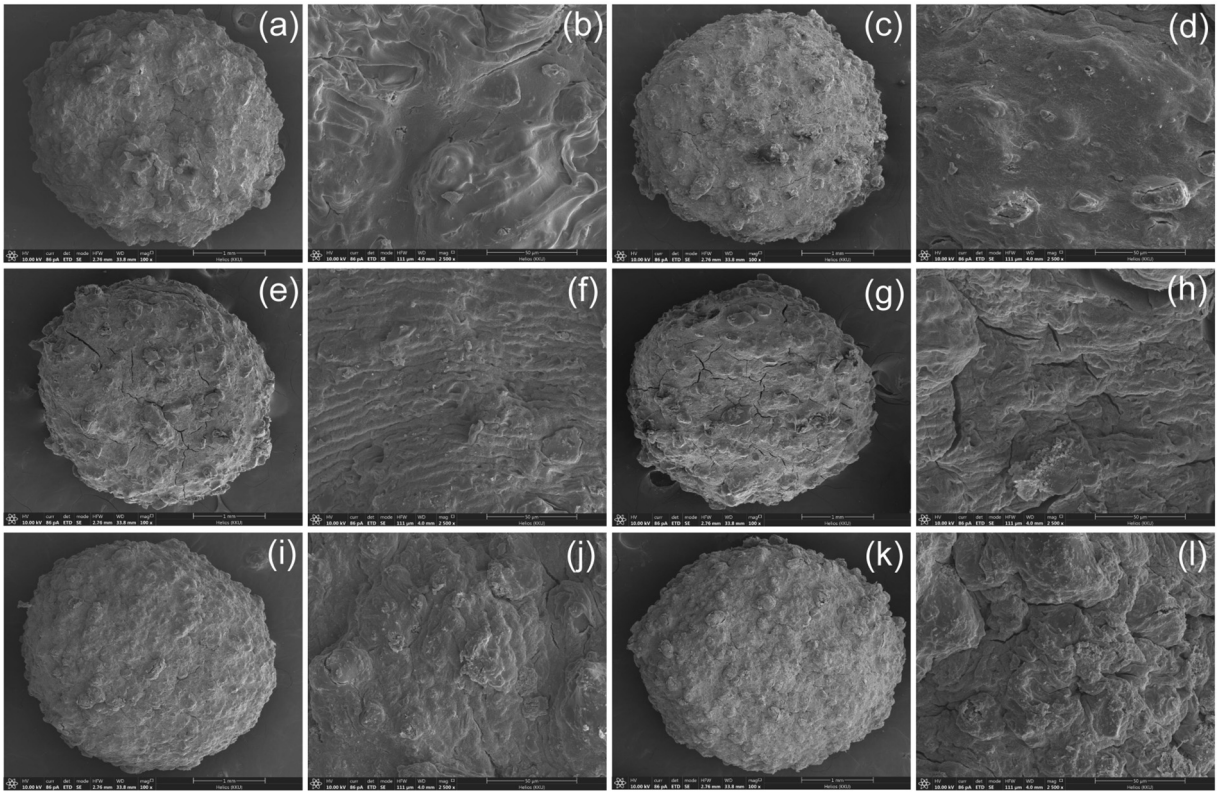

Fig. 5 FESEM-FIB images of surface morphologies in bead form at 100X magnification with 1 mm and surface at 2500X magnification with 50 μm, respectively of (a, b) chicken eggshell beads (CB), (c, d) duck eggshell beads (DB), (e, f) chicken eggshell beads mixed iron (III) oxide-hydroxide (CBF), (g, h) duck eggshell beads mixed iron (III) oxide-hydroxide (DBF), (i, j) chicken eggshell beads mixed zinc oxide (CBZ), and (k, l) duck eggshell beads mixed zinc oxide (DBZ).

Table 1 Chemical compositions of chicken eggshell beads (CB), duck eggshell beads (DB), chicken eggshell beads mixed iron (III) oxide-hydroxide (CBF), duck eggshell beads mixed iron (III) oxide-hydroxide (DBF), chicken eggshell beads mixed zinc oxide (CBZ), and duck eggshell beads mixed zinc oxide (DBZ) by EDX analysis.

Materials	Chemical element (wt%)						
	O	C	Ca	Cl	Na	Fe	Zn
CB	39.8	32.0	21.8	5.4	1.0	–	–
CBF	38.0	33.6	13.9	2.9	0.9	10.7	–
CBZ	21.3	34.2	8.0	2.3	2.5	–	31.7
DB	39.7	30. 3	22.4	6.6	1.0	–	–
DBF	40.1	36.3	12.0	5.5	1.8	4.3	–
DBZ	24.8	33.0	9.5	2.9	2.6	–	27.2

For the RB4 removal, the high RB4 adsorption efficiency should occur at the pH solution lower than the pH_{pzc} ($pH_{solution} < pH_{pzc}$) of the material because the surface of the adsorbent is positively charge. Therefore, this study should be lower than pH 7 for all dye adsorbent materials.

3.4. Batch experiments

3.4.1. The effect of dose

The effect of dose from 0.1 to 0.6 g of dye adsorbent materials with the control condition of the initial RB4 dye concentration of 50 mg/L, a sample volume of 100 mL, a contact time of 12 h, pH 7, the temperature of 50 °C, and a shaking speed of 150 rpm shown in Fig. 9a. RB4 dye removal efficiencies of all dye adsorbent materials were increased with the increase of material dosage, and their material dosages of 0.4 g, 0.4 g, 0.3 g, 0.3 g, 0.4 g, and 0.4 g demonstrated the highest RB4 dye removal efficiencies at 61.24 %, 56.56 %, 84.56 %, 75.19 %, 68.56 %, and 63.87 % for CB, DB, CBF, DBF, CBZ, and DBZ, respectively. Therefore, 0.3 g (CBF and DBF) and 0.4 g (CB, DB, CBZ, and DBZ) were the optimum dosage and were used for studying of contact time effect.

3.4.2. The effect of contact time

The effect of contact time from 3 to 18 h of dye adsorbent materials was examined with the control condition of the optimum dosage of 0.3 g (CBF and DBF) or 0.4 g (CB, DB, CBZ, and DBZ), the initial RB4 dye concentration of 50 mg/L, a

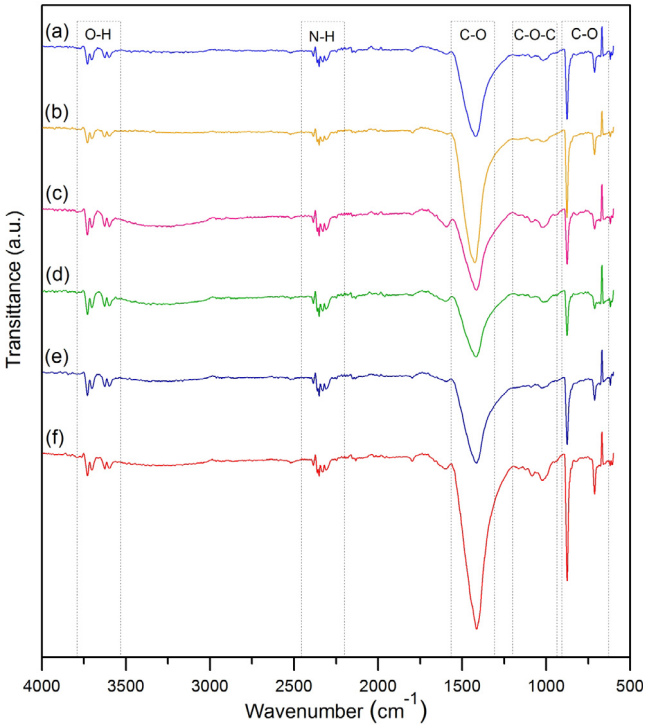

Fig. 6 FTIR spectrums of (a) chicken eggshell beads (CB), (b) duck eggshell beads (DB), (c) chicken eggshell beads mixed iron (III) oxide-hydroxide (CBF), (d) duck eggshell beads mixed iron (III) oxide-hydroxide (DBF), (e) chicken eggshell mixed zinc oxide (CBZ), and (f) duck eggshell beads mixed zinc oxide (DBZ).

sample volume of 100 mL, pH 7, the temperature of 50 °C, and a shaking speed of 150 rpm presented in Fig. 9b. RB4 dye removal efficiencies of all dye adsorbent materials were increased with the increasing of contact time. Moreover, the highest RB4 dye removal efficiencies of dye adsorbent materials were found at 12 h with 61.50 %, 57.83 %, 83.63 %, 74.62 %, 67.12 %, and 63.54 % for CB, DB, CBF, DBF, CBZ, and DBZ, respectively. Therefore, the contact time of 12 h was the optimum contact time of all dye adsorbent materials and was used for studying the temperature effect.

3.4.3. The effect of temperature

The effect of temperature from 30 to 80 °C of dye adsorbent materials was studied with the control condition of the optimum dosage of 0.3 g (CBF and DBF) or 0.4 g (CB, DB, CBZ, and DBZ), the optimum contact time of 12 h, the initial RB4 dye concentration of 50 mg/L, a sample volume of 100 mL, pH 7, and a shaking speed of 150 rpm shown in Fig. 9c. The temperature of 50 °C demonstrated the highest RB4 dye removal efficiencies of 60.44 %, 57.89 %, 85.81 %, 75.67 %, 67.07 %, and 64.56 % for CB, DB, CBF, DBF, CBZ, and DBZ, respectively. Therefore, the temperature of 50 °C was the optimum temperature for all dye adsorbent materials and was used for studying of pH effect.

3.4.4. The effect of pH

The effect of pH from 3 to 11 of dye adsorbent materials was examined with the control condition of the optimum dosage of 0.3 g (CBF and DBF) or 0.4 g (CB, DB, CBZ, and DBZ), the optimum contact time of 12 h, and the optimum temperature of 50 °C, the initial RB4 dye concentration of 50 mg/L, a sample volume of 100 mL, and a shaking speed of 150 rpm displayed in Fig. 9d. RB4 dye removal efficiencies of all dye adsorbent materials were decreased with the increasing of pH values which pH 3 demonstrated the highest RB4 dye removal efficiencies at 61.03 %, 57.67 %, 83.79 %, 74.96 %, 67.95 %, and 63.51 % for CB, DB, CBF, DBF, CBZ, and DBZ, respectively. This result also agreed with the result of the point of zero charge supported the high RB4 adsorption should occur with a pH solution $<$ pH_{pzc} of materials or a pH of solution $<$ pH 7 for all dye adsorbent materials. Moreover, the results agreed with other studies that anionic dyes were highly adsorbed at low pH or acidic pH because of the electrostatic interaction on the positively surface charged of dye adsorbent materials (Ibrahim et al., 2020). Oppositely, the increasing of pHs especially alkaline pHs affects the increasing of –OH or negatively charge sites of dye adsorbent materials, so dye removal efficiencies were decreased. Therefore, pH 3 was the optimum pH of all dye adsorbent materials and was used for the effect of concentration.

3.4.5. The effect of concentration

The effect of concentration from 30 to 90 mg/L of dye adsorbent materials was studied with the control condition of the optimum dosage of 0.3 g (CBF and DBF) or 0.4 g (CB, DB, CBZ, and DBZ), the optimum contact time of 12 h, the optimum temperature of 50 °C, and pH 3, a sample volume of 100 mL, and a shaking speed of 150 rpm reported in Fig. 9e. RB4 dye removal efficiencies from 30 to 90 mg/L of CB, DB, CBF, DBF, CBZ, and DBZ were 55.68–68.44 %, 50.16–65.70 %, 76.54–90.07 %, 95.09–85.35 %, 59.54–75.69 %,

Table 2 The chemical functional groups of chicken eggshell beads (CB), duck eggshell beads (DB), chicken eggshell beads mixed iron (III) oxide-hydroxide (CBF), duck eggshell beads mixed iron (III) oxide-hydroxide (DBF), chicken eggshell mixed zinc oxide (CBZ), and duck eggshell beads mixed zinc oxide (DBZ).

Dye adsorbent materials	Functional groups (Wavenumber (cm^{-1}))			
	O—H	N—H	C—O	C—O—C
CB	3730.24, 3637.62, 3618.31	2349.65, 2337.64	1420.48, 874.79, 712.12	1033.81
DB	3734.05, 3635.69, 3622.19	2362.41, 2322.21	1424.33, 875.57, 713.64	1037.67
CBF	3728.50, 3626.09, 3612.54	2349.68, 2327.68	1412.60, 874.48, 711.80	1033.81
DBF	3727.84, 3626.31, 3616.40	2349.67, 2328.17	1415.36, 874.77, 711.19	1035.84
CBZ	3728.26, 3625.21, 3599.73	2324.75, 2328.88	1412.67, 874.33, 711.76	1038.71
DBZ	3728.06, 3702.45, 3625.48	2383.88, 2343.43	1413.13, 874.22, 711.93	1035.74

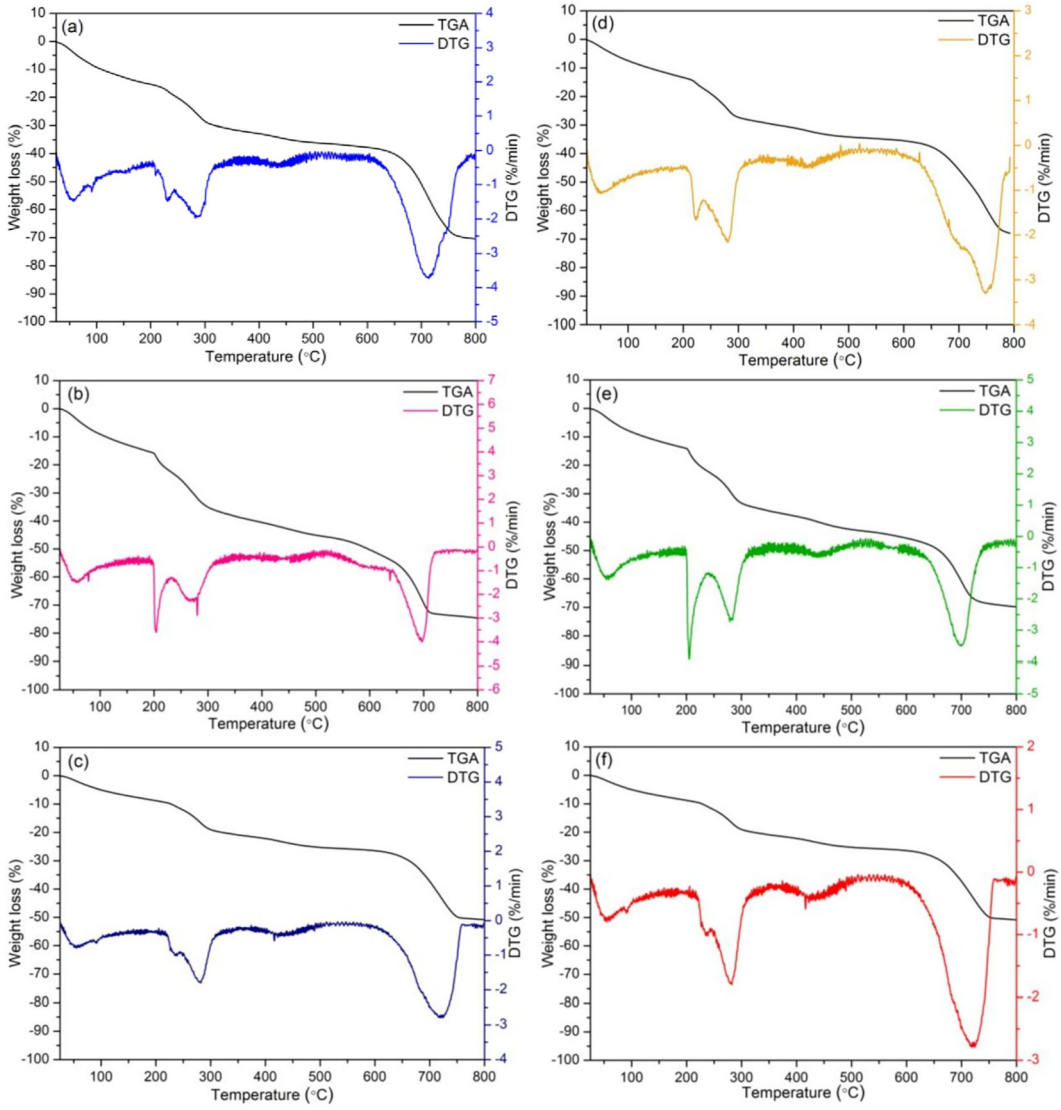

Fig. 7 TGA analysis of (a) chicken eggshell beads (CB), (b) chicken eggshell beads mixed iron (III) oxide-hydroxide (CBF), (c) chicken eggshell mixed zinc oxide (CBZ), (d) duck eggshell beads (DB), (e) duck eggshell beads mixed iron (III) oxide-hydroxide (DBF), and (f) duck eggshell beads mixed zinc oxide (DBZ).

Table 3 The weight loss of dry adsorbent materials with temperature changes in a range of 30-800 °C by TGA analysis.

Dye adsorbent materials	The weight loss (%)				
	Temperature (°C)				
	100–200	200–250	250–350	350–550	550–800
CB	15.12	4.44	11.51	5.63	33.60
CFB	15.58	7.41	15.28	8.34	27.70
CBZ	8.75	2.96	9.13	4.93	24.93
DB	13.51	8.80	13.86	6.95	26.35
DBF	12.95	4.50	11.42	5.86	33.03
DBZ	8.53	2.67	9.04	4.43	23.88

and 56.16–73.15 %, respectively which they were decreased with the increasing of RB4 dye concentration. For RB4 dye concentration of 50 mg/L, their RB4 dye removal efficiencies were 61.67 %, 56.56 %, 84.44 %, 75.22 %, 68.44 %, and 63.56 %, and CBF demonstrated the highest RB4 dye removal efficiency than others. Therefore, all dye adsorbent materials were high-quality adsorbents for dye removal of 50 mg/L in wastewater more than 56 %.

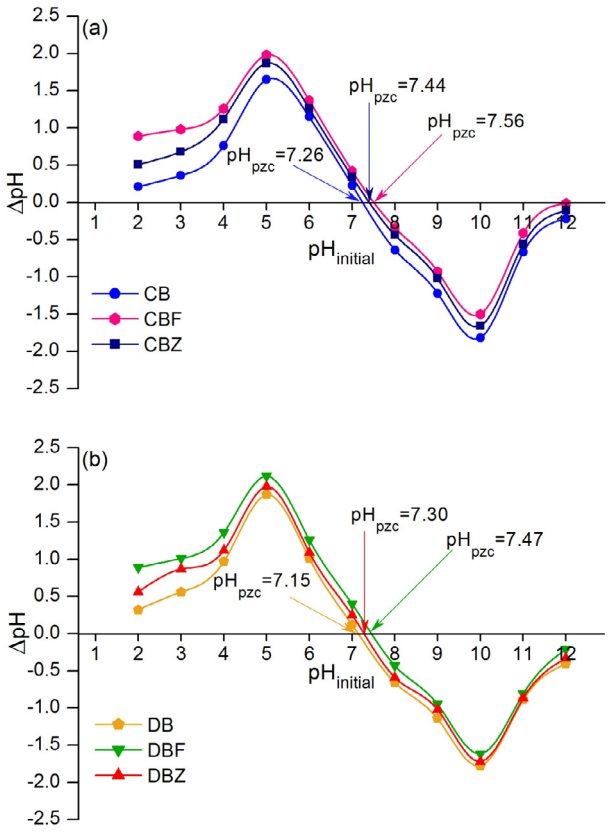

Fig. 8 The point of zero charge of (a) chicken eggshell beads (CB), chicken eggshell beads mixed iron (III) oxide-hydroxide (CBF), chicken eggshell mixed zinc oxide (CBZ) and (b) duck eggshell beads (DB), duck eggshell beads mixed iron (III) oxide-hydroxide (DBF), duck eggshell beads mixed zinc oxide (DBZ).

Finally, 0.4 g, 12 h, 50 °C, pH 3, 50 mg/L, 0.4 g, 12 h, 50 °C, pH 3, 50 mg/L, 0.3 g, 12 h, 50 °C, pH 3, 50 mg/L, 0.3 g, 12 h, 50 °C, pH 3, 50 mg/L, 0.4 g, 12 h, 50 °C, pH 3, 50 mg/L and 0.4 g, 12 h, 50 °C, pH 3, 50 mg/L, respectively were the optimum conditions in dose, contact time, temperature, pH, and concentration of CB, DB, CBF, DBF, CBZ, and DBZ, and they could be arranged in order from high to low of CBF > DBF > CBZ > DBZ > CB > DB. Therefore, the adding of iron (III) oxide-hydroxide and zinc oxide helped to improve dye removal efficiencies in all dye adsorbent materials similarly reported in other studies (Ahmadzadeh-Hakimi et al., 2017; Buthiyappan et al., 2019; Razali et al., 2020) whereas dye adsorbent materials modified with iron (III) oxide-hydroxide (CBF and DBF) demonstrated higher RB4 dye removal efficiencies than dye adsorbent materials modified with zinc oxide (CBZ and DBZ). In addition, dye adsorbent materials from chicken eggshells had higher RB4 dye removal efficiencies than dye adsorbent materials from duck eggshells. Finally, CBF demonstrated the highest RB4 dye removal efficiency than other dye adsorbent materials.

3.5. The possibility of application in real industrial wastewater treatment

The dye adsorbent materials (CB, DB, CBF, DBF, CBZ, and DBZ) could be used as adsorbents for RB4 removal in real industrial wastewater systems by running contaminated wastewater through the filter tank for treatment. After that, dye adsorbent materials were separated from treated water. From the batch experiments, approximately 0.3 g (CBF and DBF) or 0.4 g of (CB, DB, CBZ, and DBZ) were used for treating RB4 concentration of 50 mg/L in a sample volume of 100 mL with the optimum condition of a contact time of 12 h, pH 3, the temperature of 50 °C, and a shaking speed of 150 rpm. Therefore, if a sample volume of 1000 mL with the RB4 concentration of 50 mg/L, it requires the material dosages of 3 g (CBF and DBF) or 4 g (CB, DB, CBZ, and DBZ). Therefore, the RB4 concentration and wastewater volume might be used for possible consideration for wastewater treatment applications on how many the amount of dye adsorbent materials should be used.

3.6. Isotherm study

Isotherm study was used for determining of adsorption pattern of dye adsorbent materials by plotting linear and nonlinear models of Langmuir, Freundlich, Temkin, and Dubinin-Radushkevich isotherms. For linear models, Langmuir, Freundlich, Temkin, and Dubinin-Radushkevich isotherms were plotted by C_e/q_e versus C_e, log q_e versus log C_e, q_e versus ln C_e, and ln q_e versus ε^2, respectively. For nonlinear models, all isotherms were plotted by C_e versus q_e. Fig. 10a–10j demonstrated the plotting results of all isotherm models and Table 4 illustrated their equilibrium isotherm parameters.

For linear isotherm models, Langmuir maximum adsorption capacity (q_m) of CB, DB, CBF, DBF, CBZ, and DBZ were 24.096, 12.626, 30.488, 25.974, 20.408, and 19.231 mg/g, respectively, and Langmuir adsorption constants (K_L) of CB, DB, CBF, DBF, CBZ, and DBZ were 0.027, 0.030, 0.120, 0.090, 0.049, and 0.045 L/mg, respectively. For Freundlich isotherm, the $1/n$ of CB, DB, CBF, DBF, CBZ, and DBZ was 0.634, 0.567, 0.463, 0.436, 0.529, and 0.518, respectively. Freundlich adsorption constants (K_F) of CB, DB, CBF, DBF, CBZ, and DBZ were 1.222, 0.857, 5.473, 4.392, 2.013, and 1.868 $(mg/g)(L/mg)^{1/n}$, respectively. For Temkin isotherm, b_T values of CB, DB, CBF, DBF, CBZ, and DBZ were 510.744, 932.030, 391.243, 464.187, 563.101, and 605.542 (J/mol), respectively. A_T values of CB, DB, CBF, DBF, CBZ, and DBZ were 0.254, 0.271, 1.116, 0.858, 0.420, and 0.392 L/g, respectively. For the linear Dubinin-Radushkevich isotherm, the maximum adsorption capacities (q_m) of CB, DB, CBF, DBF, CBZ, and DBZ were 11.337, 6.673, 19.229, 16.651, 11.947, and 11.154 mg/g, and their activity coefficient (K_{DR}) values were 0.122, 0.129, 0.014, 0.025, 0.069, and 0.079 mol^2/J^2. In addition, their adsorption energy (E) values were 2.024, 1.970, 5.976, 4.490, 2.686, and 2.511 kJ/mol.

For nonlinear isotherm models, Langmuir maximum adsorption capacity (q_m) of CB, DB, CBF, DBF, CBZ, and DBZ were 25.123, 13.079, 30.483, 25.899, 20.623, and 19.543 mg/g, respectively, and Langmuir adsorption constants (K_L) of CB, DB, CBF, DBF, CBZ, and DBZ were 0.025, 0.028, 0.119, 0.089, 0.048, and 0.043 L/mg, respectively. For Freundlich isotherm, the $1/n$ of CB, DB, CBF, DBF, CBZ, and DBZ was 0.637, 0.581, 0.470, 0.442, 0.525, and 0.529, respectively. Freundlich adsorption constants (K_F) of CB, DB, CBF, DBF, CBZ, and DBZ were 1.212, 0.820, 5.377, 4.311, 2.040, and 1.802 $(mg/g)(L/mg)^{1/n}$, respectively. For Temkin

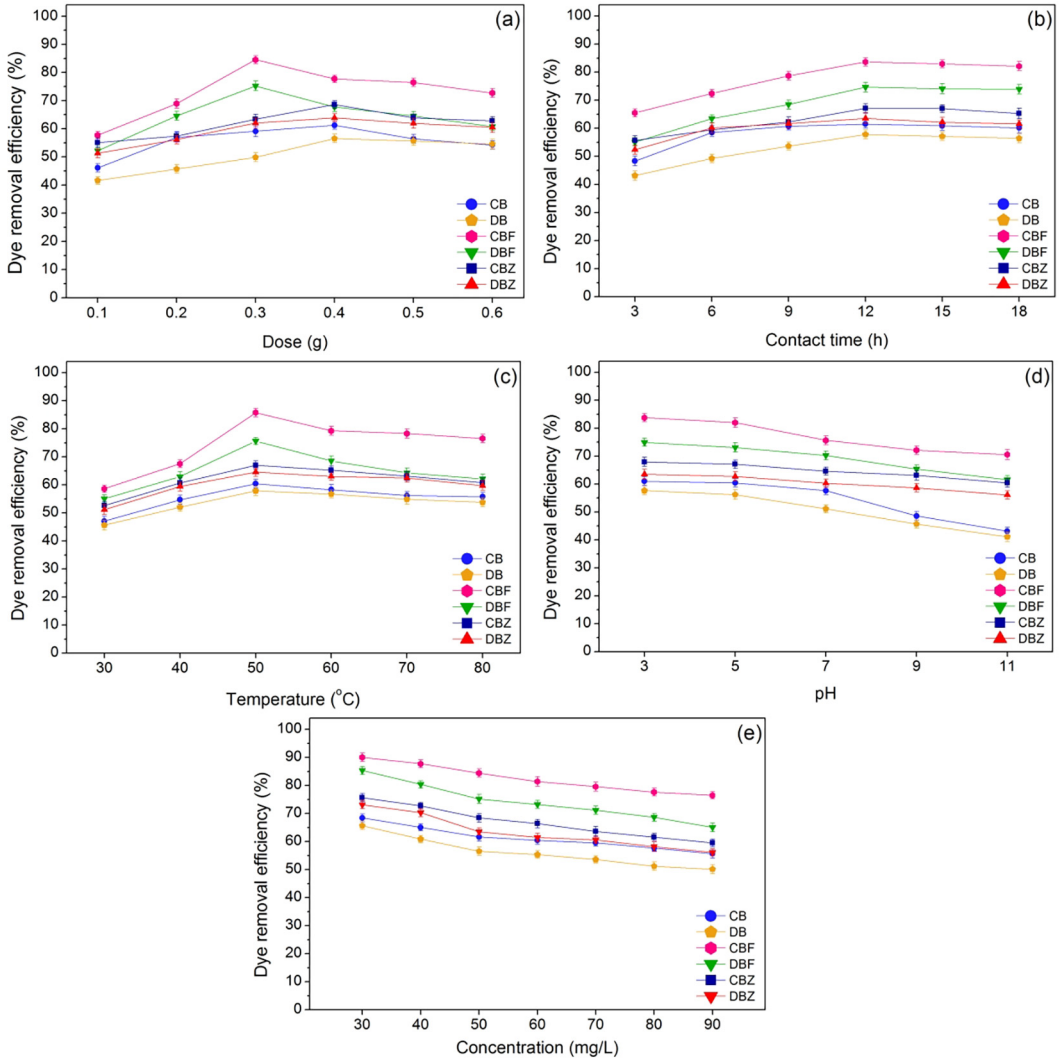

Fig. 9 The batch experiments of chicken eggshell beads (CB), duck eggshell beads (DB), chicken eggshell beads mixed iron (III) oxide-hydroxide (CBF), duck eggshell beads mixed iron (III) oxide-hydroxide (DBF), chicken eggshell beads mixed zinc oxide (CBZ), and duck eggshell beads mixed zinc oxide (BFBZ) in (a) dose, (b) contact time, (c) temperature, (d) pH, (e) concentration for dye adsorptions.

isotherm, b_T values of CB, DB, CBF, DBF, CBZ, and DBZ were 645.550, 1187.612, 492.027, 593.411, 655.516, and 806.399 (J/mol), respectively. A_T values of CB, DB, CBF, DBF, CBZ, and DBZ were 0.352, 0.400, 1.739, 1.429, 0.541 and 0.655 L/g, respectively. For the nonlinear Dubinin-Radushkevich isotherm, the maximum adsorption capacities (q_m) of CB, DB, CBF, DBF, CBZ, and DBZ were 9.599, 5.695, 16.349, 14.207, 10.368, and 9.440 mg/g, and their activity coefficient (K_{DR}) values were 0.094, 0.097, 0.011, 0.019, 0.055, and 0.058 mol^2/J^2. In addition, their adsorption energy (E) values were 2.307, 2.267, 6.810, 5.183, 30.28, and 2.944 kJ/mol.

For R^2 value consideration, R^2 values of CB, DB, CBF, DBF, CBZ, and DBZ in linear Langmuir model were 0.971, 0.965, 0.975, 0.979, 0.989, and 0.961, respectively, and linear Freundlich model were 0.997, 0.995, 0.997, 0.993, 0.998, and 0.988, respectively. R^2 values of CB, DB, CBF, DBF, CBZ, and DBZ in linear Temkin model were 0.977, 0.937, 0.973, 0.970, 0.923, and 0.965, respectively, and linear Dubinin-Radushkevich model were 0.856, 0.827, 0.824, 0.773, 0.869, and 0.836, respectively. In addition, R^2 values of CB, DB, CBF, DBF, CBZ, and DBZ in nonlinear Langmuir model were 0.992, 0.983, 0.969, 0.966, 0.991, and 0.970, respectively, and nonlinear Freundlich model were 0.996, 0.996, 0.996, 0.992, 0.999, and 0.989, respectively. R^2 values of CB, DB, CBF, DBF, CBZ, and DBZ in nonlinear Temkin model were 0.994, 0.989, 0.971, 0.989, 0.996, and 0.946, respectively, and nonlinear Dubinin-Radushkevich model were 0.854, 0.829, 0.833, 0.772, 0.872, and 0.823, respectively.

Moreover, R^2_{adj} of CB, DB, CBF, DBF, CBZ, and DBZ in nonlinear Langmuir model were 0.991, 0.980, 0.963, 0.959, 0.989, and 0.964, respectively, and R^2_{adj} of CB, DB, CBF, DBF, CBZ, and DBZ in nonlinear Freundlich model were 0.996, 0.995, 0.996, 0.991, 0.998, and 0.987, respectively. R^2_{adj} of CB, DB, CBF, DBF, CBZ, and DBZ in nonlinear Temkin model were 0.993, 0.987, 0.965, 0.987, 0.996, and 0.935, respectively, and R^2_{adj} of CB, DB, CBF, DBF, CBZ, and DBZ in nonlinear Dubinin-Radushkevich model were 0.825, 0.794, 0.799, 0.727, 0.846, and 0.788, respectively.

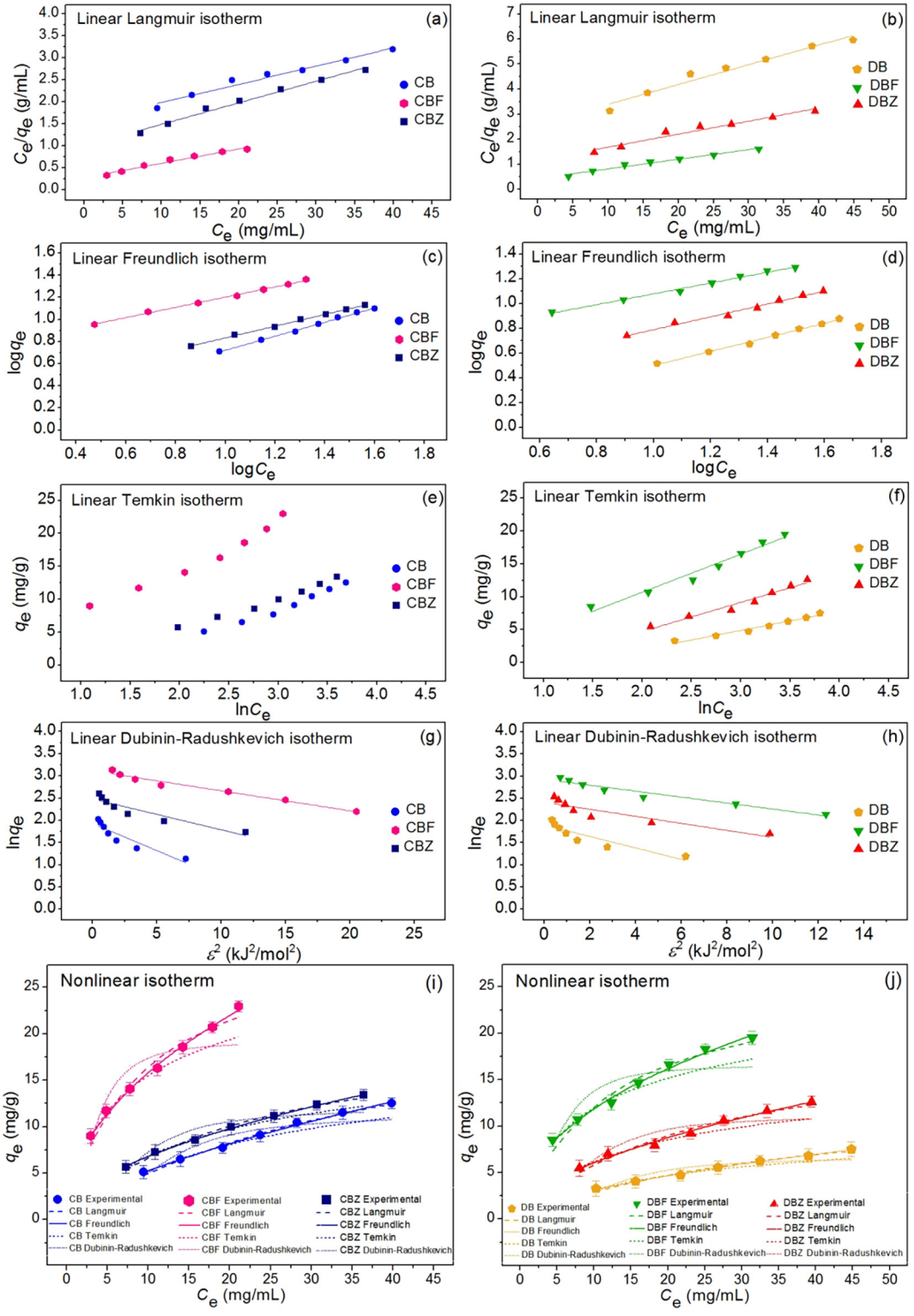

Fig. 10 (a and b) linear Langmuir, (c and d) linear Freundlich, (e and f) linear Temkin, (g and h) linear Dubinin-Radushkevich, and (i and j) nonlinear adsorption isotherms of chicken eggshell beads (CB), duck eggshell beads (DB), chicken eggshell beads mixed iron (III) oxide-hydroxide (CBF), duck eggshell beads mixed iron (III) oxide-hydroxide (DBF), chicken eggshell beads mixed zinc oxide (CBZ), and duck eggshell beads mixed zinc oxide (DBZ) for dye adsorptions.

Since R^2 values of CB, DB, CBF, DBF, CBZ, and DBZ in both linear and nonlinear Freundlich models were higher than Langmuir, Temkin, and Dubinin-Radushkevich models, their adsorption patterns corresponded to Freundlich isotherm with relating to physiochemical adsorption. Finally, since the equilibrium parameters and R^2 values of CB, DB, CBF, DBF, CBZ, and DBZ on dye adsorptions by linear and nonlinear Langmuir, Freundlich, Temkin, and Dubinin-Radushkevich

Table 4 The equilibrium isotherm parameters of chicken eggshell beads (CB), duck eggshell beads (DB), chicken eggshell beads mixed iron (III) oxide-hydroxide (CBF), duck eggshell beads mixed iron (III) oxide-hydroxide (DBF), chicken eggshell beads mixed zinc oxide (CBZ), and duck eggshell beads mixed zinc oxide (DBZ) for dye adsorptions.

Isotherm model	Parameter	CB	DB	CBF	DBF	CBZ	DBZ
Linear							
Langmuir	q_m (mg/g)	24.096	12.626	30.488	25.974	20.408	19.231
	K_L (L/mg)	0.027	0.030	0.120	0.090	0.049	0.045
	R^2	0.971	0.965	0.975	0.979	0.989	0.961
Freundlich	K_F (mg/g)(L/mg)$^{1/n}$	1.222	0.857	5.473	4.392	2.013	1.868
	$1/n$	0.634	0.567	0.463	0.436	0.529	0.518
	R^2	0.997	0.995	0.997	0.993	0.998	0.988
Temkin	b_T (J/mol)	510.744	932.030	391.243	464.187	563.101	605.542
	A_T (L/g)	0.254	0.271	1.116	0.858	0.420	0.392
	R^2	0.977	0.937	0.973	0.970	0.923	0.965
Dubinin-Radushkevich	q_m (mg/g)	11.337	6.673	19.229	16.651	11.947	11.154
	K_{DR} (mol^2/J^2)	0.122	0.129	0.014	0.025	0.069	0.079
	E (kJ/mol)	2.024	1.970	5.976	4.490	2.686	2.511
	R^2	0.856	0.827	0.824	0.773	0.869	0.836
Nonlinear							
Langmuir	q_m (mg/g)	25.123	13.079	30.483	25.899	20.623	19.543
	K_L (L/mg)	0.025	0.028	0.119	0.089	0.048	0.043
	R^2	0.992	0.983	0.969	0.966	0.991	0.970
	R^2_{adj}	0.991	0.980	0.963	0.959	0.989	0.964
	RMSE	0.262	0.219	0.953	0.821	0.286	0.490
Freundlich	K_F (mg/g)(L/mg)$^{1/n}$	1.212	0.820	5.377	4.311	2.040	1.802
	$1/n$	0.637	0.581	0.470	0.442	0.525	0.529
	R^2	0.996	0.996	0.996	0.992	0.999	0.989
	R^2_{adj}	0.996	0.995	0.996	0.991	0.998	0.987
	RMSE	0.177	0.108	0.327	0.387	0.109	0.294
Temkin	b_T (J/mol)	645.550	1187.612	492.027	593.411	655.516	806.399
	A_T (L/g)	0.352	0.400	1.739	1.429	0.541	0.655
	R^2	0.994	0.989	0.971	0.989	0.996	0.946
	R^2_{adj}	0.993	0.987	0.965	0.987	0.996	0.935
	RMSE	0.971	0.575	1.771	1.566	0.676	1.117
Dubinin-Radushkevich	q_m (mg/g)	9.599	5.695	16.349	14.207	10.368	9.440
	K_{DR} (mol^2/J^2)	0.094	0.097	0.011	0.019	0.055	0.058
	E (kJ/mol)	2.307	2.267	6.810	5.183	3.028	2.944
	R^2	0.854	0.829	0.833	0.772	0.872	0.823
	R^2_{adj}	0.825	0.794	0.799	0.727	0.846	0.788
	RMSE	2.014	1.195	2.613	2.310	1.955	2.073

isotherm models had approximately closely values, their results were consistent with each other. Therefore, both linear and nonlinear isotherm models were required to plot graphs for the protection of data mistranslation (Ngamsurach and Praipipat, 2021, 2022; Threepanich and Praipipat, 2022).

Finally, the maximum dye adsorption capacity (q_m) of this study was compared with other adsorbents for RB4 dye removal reported in Table 5. The q_m values of all dye adsorbent materials in this study had higher than the pecan nut shells and chitosan glutaraldehyde-crosslinked beads (Aguayo-Villarreal et al., 2013; Galan et al., 2021). In addition, they had higher or lower q_m values than other studies which might be from the different adsorbents and laboratory conditions shown in Table 5. However, CBF which represented the highest RB4 dye removal in this study still had a higher q_m value than many studies reported in Table 5.

3.7. Kinetic study

A kinetic study was designed to explain the adsorption rate and mechanism of dye adsorbent materials by using linear and nonlinear kinetic models of pseudo-first-order, pseudo-second-order, elovich, and intra-particle diffusion. For linear models, pseudo-first-order kinetic, pseudo-second-order kinetic, elovich, and intra-particle diffusion were plotted by $\ln(q_e\text{-}q_t)$ versus time (t), t/q_t versus time (t), q_t versus ln t, and q_t versus time ($t^{0.5}$), respectively. For nonlinear models, all kinetic models were plotted by q_t versus time (t). Fig. 11a–11j demonstrated the plotting results of all kinetic models and Table 6 illustrated their adsorption kinetic parameters.

For linear kinetic models, the adsorption capacity (q_e) of pseudo-first-order kinetic model of CB, DB, CBF, DBF, CBZ, and DBZ were 2.476, 1.884, 4.298, 3.183, 3.766, and 5.667 mg/g, respectively, and the reaction of rate constants of pseudo-first-order kinetic model (k_1) of CB, DB, CBF, DBF, CBZ, and DBZ were 0.003, 0.001, 0.005, 0.004, 0.001, and 0.001 min^{-1}, respectively. For pseudo-second-order kinetic model, the adsorption capacity (q_e) of CB, DB, CBF, DBF, CBZ, and DBZ were 7.874, 4.847, 14.388, 12.755, 8.658, and 8.052 mg/g, respectively, and the reaction of rate constants of pseudo-second-order kinetic model (k_2) of CB,

Table 5 Comparison of the maximum dye adsorption capacity (q_m) with various adsorbents for RB4 dye removal.

Adsorbents	q_m (mg/g)	References
Bokbunja waste seeds untreated with *n*-hexane	25.44	(Binupriya et al., 2009)
Bokbunja waste seeds treated with *n*-hexane	26.16	
Barley straw modified with hexadecylpyridinium chloride monohydrate	29.16	(Ibrahim et al., 2010b)
Barley straw modified with NaOH and hexadecylpyridinium chloride monohydrate	31.50	(Ibrahim et al., 2010a)
Peanut shell modified with ionic liquid	30.20	(Lawal et al., 2017)
Peanut shell activated carbon modified with ionic liquid	376.25	
Picea abies Karst. bark with $ZnCl_2$	59.00	(Dos Reis et al., 2021)
Picea abies Karst. bark with KOH	339.15	
Mustard stalk activated carbon	25.80	(Ullhyan, 2014)
Bagasse modified propionic acid	13.20	(Said et al., 2013)
Pecan nut shells	7.91	(Aguayo-Villarreal et al., 2013)
Chitosan glutaraldehyde-crosslinked beads	1.76	(Galan et al., 2021)
CB	24.10	This study
DB	12.63	This study
CBF	30.49	This study
DBF	25.97	This study
CBZ	20.41	This study
DBZ	19.23	This study

DB, CBF, DBF, CBZ, and DBZ were 0.003, 0.006, 0.002, 0.003, 0.003, and 0.004 g/mg·min, respectively. For elovich model, the initial adsorption rates (α) of CB, DB, CBF, DBF, CBZ, and DBZ were 0.192, 2.894, 0.510, 0.402, 0.190, and 0.110 mg/g/min, respectively, and the extents of surface coverage (β) of CB, DB, CBF, DBF, CBZ, and DBZ were 0.881, 1.445, 0.484, 0.545, 0.813, and 0.859 g/mg, respectively. For intra-particle diffusion model, the reaction of rate constants of intra-particle diffusion model (k_i) of CB, DB, CBF, DBF, CBZ, and DBZ were 0.105, 0.052, 0.132, 0.105, 0.100, and 0.092 mg/g·min $^{0.5}$, respectively, and the constant C_i values of CB, DB, CBF, DBF, CBZ, and DBZ were 4.769, 3.257, 10.372, 9.582, 5.599, and 5.335 (mg/g), respectively.

For nonlinear kinetic models, the adsorption capacity (q_e) of pseudo-first-order kinetic model of CB, DB, CBF, DBF, CBZ, and DBZ were 2.671, 2.033, 4.637, 3.434, 4.064, and 6.115 mg/g, respectively, and the reaction of rate constants of pseudo-first-order kinetic model (k_1) of CB, DB, CBF, DBF, CBZ, and DBZ were 0.005, 0.001, 0.006, 0.006, 0.001, and 0.001 min^{-1}, respectively. For pseudo-second-order kinetic model, the adsorption capacity (q_e) of CB, DB, CBF, DBF, CBZ, and DBZ were 7.721, 4.665, 13.987, 12.338, 8.271, and 7.876 mg/g, respectively, and the reaction of rate constants of pseudo-second-order kinetic model (k_2) of CB, DB, CBF, DBF, CBZ, and DBZ were 0.004, 0.009, 0.004, 0.005, 0.005, and 0.005 g/mg·min, respectively. For elovich model, the initial adsorption rates (α) of CB, DB, CBF, DBF, CBZ, and DBZ were 0.215, 2.746, 0.846, 0.437, 0.182, and 0.127 mg/g/min, respectively, and the extents of surface coverage (β) of CB, DB, CBF, DBF, CBZ, and DBZ were 0.806, 1.463, 0.560, 0.548, 0.844, and 0.809 g/mg, respectively. For intra-particle diffusion model, the reaction of rate constants of intra-particle diffusion model (k_i) of CB, DB, CBF, DBF, CBZ, and DBZ were 0.212, 0.125, 0.364, 0.320, 0.225, and 0.211 mg/g·min $^{0.5}$, respectively, and the constant C_i values of CB, DB, CBF, DBF, CBZ, and DBZ were 2.323, 1.734, 5.521, 5.101, 2.981, and 2.840 mg/g, respectively.

For R^2 value consideration, R^2 values of CB, DB, CBF, DBF, CBZ, and DBZ in linear pseudo-first-order kinetic model were 0.829, 0.881, 0.822, 0.705, 0.863, and 0.796, respectively, and linear pseudo-second-order kinetic model were 0.999, 0.999, 0.999, 0.999, 0.998, and 0.999, respectively. R^2 values of CB, DB, CBF, DBF, CBZ, and DBZ in linear elovich model were 0.987, 0.972, 0.958, 0.946, 0.974, and 0.978, respectively, and linear intra-particle model were 0.876, 0.932, 0.948, 0.930, 0.925, and 0.885, respectively. In addition, R^2 values of CB, DB, CBF, DBF, CBZ, and DBZ in nonlinear pseudo-first-order kinetic model were 0.881, 0.882, 0.826, 0.706, 0.862, and 0.798, respectively, and nonlinear pseudo-second-order kinetic model were 0.998, 0.997, 0.998, 0.998, 0.997, and 0.998, respectively. R^2 values of CB, DB, CBF, DBF, CBZ, and DBZ in nonlinear elovich model were 0.988, 0.974, 0.961, 0.948, 0.979, and 0.982, respectively, and nonlinear intra-particle diffusion model were 0.873, 0.931, 0.948, 0.931, 0.927, and 0.884, respectively.

Moreover, R^2_{adj} of CB, DB, CBF, DBF, CBZ, and DBZ in nonlinear pseudo-first-order kinetic model were 0.866, 0.867, 0.805, 0.669, 0.845, and 0.772, respectively, and R^2_{adj} of CB, DB, CBF, DBF, CBZ, and DBZ in nonlinear pseudo-second-order kinetic model were 0.997, 0.996, 0.998, 0.998, 0.997, and 0.998, respectively. R^2_{adj} of CB, DB, CBF, DBF, CBZ, and DBZ in nonlinear elovich model were 0.986, 0.971, 0.956, 0.942, 0.976, and 0.980, respectively, and nonlinear intra-particle diffusion model were 0.857, 0.923, 0.942, 0.922, 0.918, and 0.870, respectively.

Since R^2 values of CB, DB, CBF, DBF, CBZ, and DBZ in both linear and nonlinear pseudo-second-order kinetic models were higher than pseudo-first-order kinetic, elovich, and intra-particle diffusion models, their adsorption rate and mechanism of all dye adsorbent materials corresponded to pseudo-second-order kinetic model with relating to chemisorption process with heterogenous adoption. Finally, the results of both linear and nonlinear pseudo-first-order, pseudo-second-order kinetic, elovich, and intra-particle models of all dye adsorbent materials were consistent with each other, so the plotting of both linear and nonlinear kinetic models was also recommended for correctly data translations (Ngamsurach and Praipipat, 2021, 2022; Threepanich and Praipipat, 2022).

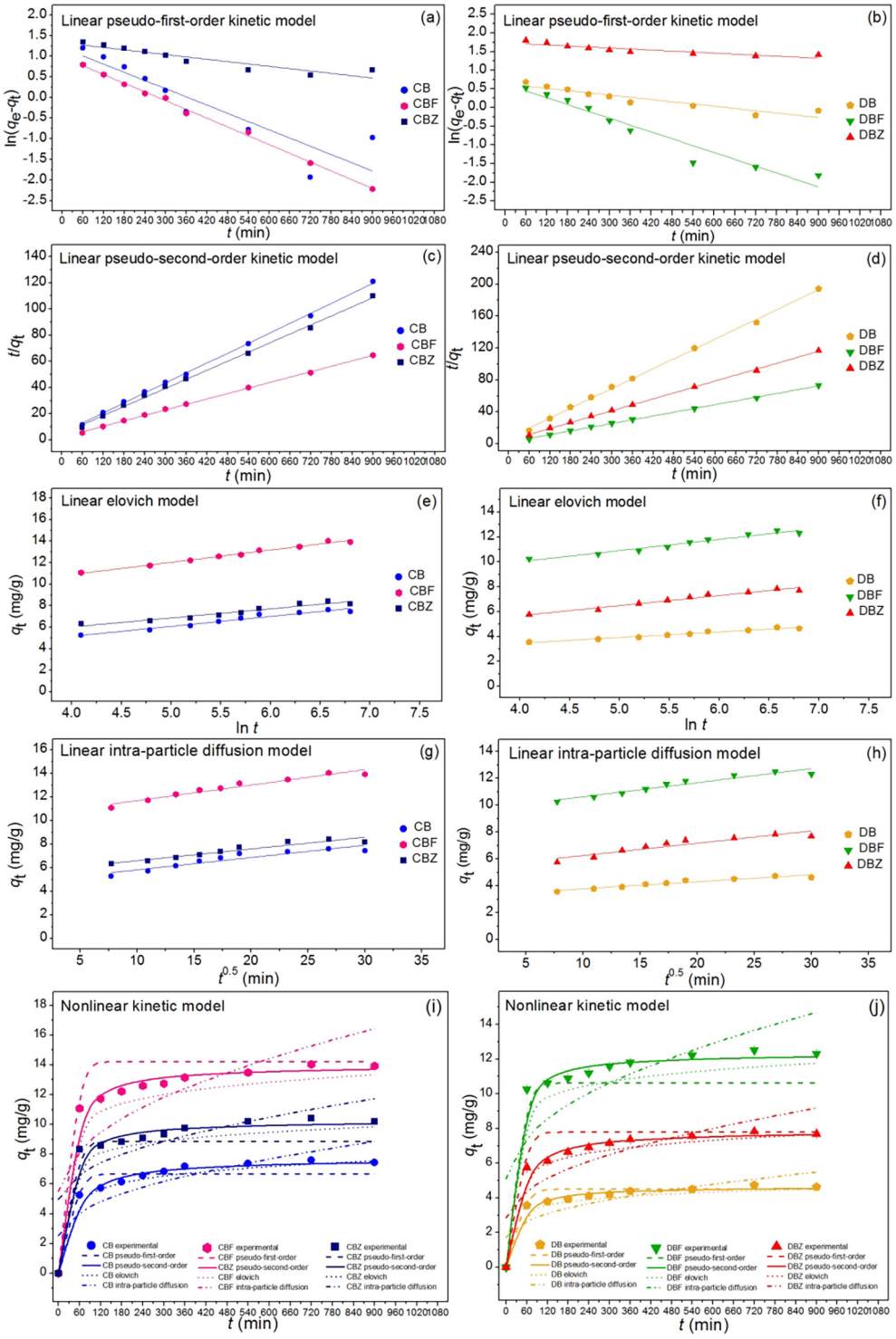

Fig. 11 (a and b) linear pseudo-first-order, (c and d) linear pseudo-second-order, (e and f) linear elovich, and (g and h) linear intra-particle diffusion, and (i and j) nonlinear kinetic models of chicken eggshell beads (CB), duck eggshell beads (DB), chicken eggshell beads mixed iron (III) oxide-hydroxide (CBF), duck eggshell beads mixed iron (III) oxide-hydroxide (DBF), chicken eggshell beads mixed zinc oxide (CBZ), and duck eggshell beads mixed zinc oxide (DBZ) for dye adsorptions.

3.8. Thermodynamic study

The thermodynamic studies were conducted to investigate the effect of temperature in a range of 30-80 °C or 303–353 K on dye adsorbent materials for RB4 dye adsorption, and the results are demonstrated in Table 7. All dye adsorbent materials had the negative value of $\Delta G°$ in a temperature range of 303–323 K which indicated the adsorption of RB4 onto them was a spontaneous nature and favorable process. This result corresponded to the batch experiment found the optimum tem-

Table 6 The adsorption kinetic parameters of chicken eggshell beads (CB), duck eggshell beads (DB), chicken eggshell beads mixed iron (III) oxide-hydroxide (CBF), duck eggshell beads mixed iron (III) oxide-hydroxide (DBF), chicken eggshell beads mixed zinc oxide (CBZ), and duck eggshell beads mixed zinc oxide (DBZ) for dye adsorptions.

Kinetic model	Parameter	CB	DB	CBF	DBF	CBZ	DBZ
Linear							
Pseudo-first-order	q_e (mg/g)	2.476	1.884	4.298	3.183	3.766	5.667
	k_1 (min^{-1})	0.003	0.001	0.005	0.004	0.001	0.001
	R^2	0.829	0.881	0.822	0.705	0.863	0.796
Pseudo-second-order	q_e (mg/g)	7.874	4.847	14.388	12.755	8.658	8.052
	k_1 (min^{-1})	0.003	0.006	0.002	0.003	0.003	0.004
	R^2	0.999	0.999	0.999	0.999	0.998	0.999
Elovich	α (mg/g/min)	0.192	2.894	0.510	0.402	0.190	0.110
	β (g/mg)	0.881	1.445	0.484	0.545	0.813	0.859
	R^2	0.987	0.972	0.958	0.946	0.974	0.978
Intra-particle diffusion	k_i (mg/g•$min^{0.5}$)	0.105	0.052	0.132	0.105	0.100	0.092
	C_i (mg/g)	4.769	3.257	10.372	9.582	5.599	5.335
	R^2	0.876	0.932	0.948	0.930	0.925	0.885
Nonlinear							
Pseudo-first-order	q_e (mg/g)	2.671	2.033	4.637	3.434	4.064	6.115
	k_1 (min^{-1})	0.005	0.001	0.006	0.006	0.001	0.001
	R^2	0.881	0.882	0.826	0.706	0.862	0.798
	R^2_{adj}	0.866	0.867	0.805	0.669	0.845	0.772
	RMSE	0.822	0.509	1.832	2.135	0.966	1.105
Pseudo-second-order	q_e (mg/g)	7.721	4.665	13.987	12.338	8.271	7.876
	k_2 (g/mg•min)	0.004	0.009	0.004	0.005	0.005	0.005
	R^2	0.998	0.997	0.998	0.998	0.997	0.998
	R^2_{adj}	0.997	0.996	0.998	0.998	0.997	0.998
	RMSE	0.238	0.152	0.364	0.349	0.354	0.207
Elovich	α (mg/g/min)	0.215	2.746	0.846	0.437	0.182	0.127
	β (g/mg)	0.806	1.463	0.560	0.548	0.844	0.809
	R^2	0.988	0.974	0.961	0.948	0.979	0.982
	R^2_{adj}	0.986	0.971	0.956	0.942	0.976	0.980
	RMSE	0.265	0.237	0.871	0.894	0.379	0.331
Intra-particle diffusion	k_i (mg/g•$min^{0.5}$)	0.212	0.125	0.364	0.320	0.225	0.211
	C_i (mg/g)	2.323	1.734	5.521	5.101	2.981	2.840
	R^2	0.873	0.931	0.948	0.931	0.927	0.884
	R^2_{adj}	0.857	0.923	0.942	0.922	0.918	0.870
	RMSE	1.264	0.846	2.685	2.481	1.459	1.397

Table 7 Thermodynamic parameters of chicken eggshell beads (CB), duck eggshell beads (DB), chicken eggshell beads mixed iron (III) oxide-hydroxide (CBF), duck eggshell beads mixed iron (III) oxide-hydroxide (DBF), chicken eggshell beads mixed zinc oxide (CBZ), and duck eggshell beads mixed zinc oxide (DBZ).

Dye adsorbent materials	$\Delta G°$ (kJ/mol)						$\Delta H°$ (kJ/mol)	$\Delta S°$ (kJ/mol K)
	303 K	313 K	323 K	333 K	343 K	353 K		
CB	−1.14	−0.58	−0.02	0.54	1.10	1.66	−18.12	−0.06
DB	−1.13	−0.57	−0.01	0.55	1.11	1.66	−18.05	−0.06
CBF	−3.45	−2.76	−2.08	−1.39	−0.71	−0.02	−24.23	−0.07
DBF	−2.92	−2.34	−1.76	−1.18	−0.59	−0.01	−20.58	−0.06
CBZ	−2.45	−1.86	−1.27	−0.67	−0.08	0.51	−20.42	−0.06
DBZ	−2.08	−1.53	−0.97	−0.42	0.13	0.68	−18.79	−0.06

perature of 50 °C or 323 K offering the highest RB4 dye removal in all materials. In addition, their $\Delta G°$ values increased with the increase in temperature which showed a less favorable process of RB4 adsorption. For their $\Delta H°$ and $\Delta S°$ values, these values had negative values in all dye adsorbent materials which indicated their RB4 adsorption processes were exothermic in nature with the decrease in the degree of randomness during the adsorption process (Mukesh Kumar et al., 2019). Therefore, the increase in temperature was not favorable for RB4 adsorption onto dye adsorbent materials.

4. The possible mechanism of RB4 adsorption onto dye adsorbent materials

Fig. 12 demonstrated the possible mechanism of RB4 dye adsorption onto dye adsorbent materials of CB, DB, CBF,

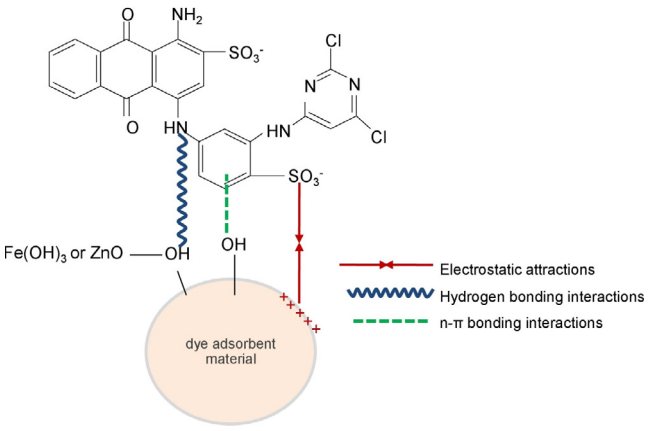

Fig. 12 Schematic diagram of the possible mechanism of RB4 dye adsorption by dye adsorbent materials.

DBF, CBZ, and DBZ. The result of FTIR illustrated the main functional groups of O—H, N—H, C—O, and C—O—C in all dye adsorbent materials, and they play an important role in RB4 absorption. In addition, the complex molecules of iron (III) oxide-hydroxide ($Fe(OH)_3$) or zinc oxide (ZnO) with a hydroxyl group (–OH) through sharing electrons also occurred in materials by adding $Fe(OH)_3$ or ZnO (CBF, DBF, CBZ, and DBZ) (Gupta and Nayak, 2012). Three possible reactions of electrostatic interactions, hydrogen bonding interactions, and n-π bonding interactions might be the main mechanism of RB4 dye adsorptions on dye adsorbent materials (Galan et al., 2021). Firstly, the electrostatic interactions might occur from the interaction between the negatively charged sulfonate groups ($–SO_3^-$) of RB4 dye molecules and the positively charged hydroxy group (–OH) on the surface of dye adsorbent materials at acid pH or pH < pH_{pzc} (Awasthi et al., 2020). Secondly, the hydrogen bonding interactions might be from the capturing of the nitrogen (N) of the RB4 dye molecule by the hydrogen ions (H^+) of a hydroxyl group (–OH) (Ma et al., 2021). Finally, the n-π bonding interactions might be from the capturing of the aromatic rings of RB4 dye molecules by the hydroxyl group (–OH) or oxygen bond (–O) in dye adsorbent materials (Awasthi et al., 2020).

5. Conclusions

Chicken eggshell beads (CB), duck eggshell beads (DB), chicken eggshell beads mixed iron (III) oxide-hydroxide (CBF), duck eggshell beads mixed iron (III) oxide-hydroxide (DBF), chicken eggshell beads mixed zinc oxide (CBZ), and duck eggshell beads mixed zinc oxide (DBZ) were synthesized for RB4 removal in an aqueous solution. Six dye adsorbent materials had a spherical shape with dark or light-cream beaded color or iron-rust beaded color. All dye adsorbent materials demonstrated semi-crystalline structures with specific peaks of calcium carbonate, sodium alginate, and the specified peaks of iron (III) oxide-hydroxide and zinc oxide were found in CBF, DBF, CBZ, and DBZ. Their surface morphologies had spherical shapes with coarse surfaces, and chemical elements of oxygen (O), carbon (C), calcium (Ca), chlorine (Cl), and sodium (Na) were found in all dye adsorbent materials whereas iron (Fe) and zinc (Zn) were found only dye adsorbent materials modified with iron (III) oxide-hydroxide or zinc oxide. Four main function groups of O—H, N—H, C—O, and C—O—C were detected in all materials. For TGA and DTG analysis, their results indicated the temperature was an important effect to change weight loss of a temperature range from 30 to 800 °C in all dye adsorbent materials with occurring both endothermic and exothermic processes for removing moisture contents and decompositions of organic functional groups or calcium carbonate ($CaCO_3$) in materials. The optimum conditions of CB, DB, CBF, DBF, CBZ, and DBZ on RB4 dye adsorptions of 50 mg/L were 0.4 g, 12 h, 50 °C, pH 3, 0.4 g, 12 h, 50 °C, pH 3, 0.3 g, 12 h, 50 °C, pH 3, 0.3 g, 12 h, 50 °C, pH 3, 0.4 g, 12 h, 50 °C, pH 3, and 0.4 g, 12 h, 50 °C, pH 3, respectively, and they could be arranged in order from high to low of CBF > DBF > CBZ > DBZ > CB > DB which they could remove RB4 dye more than 56 %. Especially, CBF had the highest RB4 removal efficiency of 84.44 %. As a result, adding iron (III) oxide-hydroxide and zinc oxide helped to improve RB4 dye adsorbent efficiencies which an iron (III) oxide-hydroxide increased RB4 removal efficiency of chicken and duck eggshell beads more than zinc oxide. The point of zero charge (pH_{pzc}) of dye adsorbent materials was in a range of pH 7–8 indicating their high RB4 adsorptions should be found at the pH of solution < pH_{pzc} with the positively charged surface. This result corresponded to the result of the pH effect that the highest RB4 dye removal was found at a pH of 3 in all dye adsorbent materials. For adsorption isotherms and kinetics, they corresponded Freundlich model and pseudo-second-order kinetic models relating to physiochemical adsorption and chemisorption process. The maximum adsorption capacities (q_m) of CB, DB, CBF, DBF, CBZ, and DBZ were 24.096, 12.626, 30.488, 25.974, 20.408, and 19.231 mg/g, respectively, and they could be arranged in order from high to low in CBF > DBF > CBZ > DBZ > CB > DB. For the thermodynamic study, since the $\Delta G°$ values of all dye adsorbent materials had negative values, the adsorptions of RB4 onto dye adsorbent materials were a spontaneous nature and favorable process. In addition, their $\Delta H°$ and $\Delta S°$ values had also negative values, so their RB4 adsorption processes were exothermic in nature with a decrease in the degree of randomness during the adsorption process. As a result, the increase in temperature was not favorable for RB4 adsorption onto dye adsorbent materials. The RB4 adsorption mechanism of all dye adsorbent materials might be described by three possible reactions of electrostatic interactions, hydrogen bonding interactions, and n-π bonding. Therefore, all dye adsorbent materials are potential materials for RB4 dye adsorptions in an aqueous solution, and they might be used for industrial applications in the future. For future works, desorption experiments are required for studying the possible reuse of materials, and continuous flow study is also needed for real industrial wastewater treatment applications.

CRediT authorship contribution statement

Pornsawai Praipipat: Supervision, Conceptualization, Funding acquisition, Investigation, Methodology, Validation, Visualization, Writing – original draft, Writing – review & editing. **Pimploy Ngamsurach:** Visualization, Writing – original draft. **Chonthicha Saekrathok:** Investigation. **Sukanya Phomtai:** Investigation.

Data availability

The raw/processed data required to reproduce these findings cannot be shared at this time due to legal or ethical reasons. The raw/processed data required to reproduce these findings cannot be shared at this time as the data also forms part of an ongoing study.

Declaration of Competing Interest

The authors declare that they have no known competing financial interests or personal relationships that could have appeared to influence the work reported in this paper.

Acknowledgments

The authors are grateful for the financial support from The Office of the Higher Education Commission and The Thailand Research Fund grant (MRG6080114), Coordinating Center for Thai Government Science and Technology Scholarship Students (CSTS) and National Science and Technology Development Agency (NSTDA) Fund grant (SCHNR2016-122), and Research and Technology Transfer Affairs of Khon Kaen University.

References

Aguayo-Villarreal, I.A., Ramírez-Montoya, L.A., Hernández-Montoya, V., Bonilla-Petriciolet, A., Montes-Morán, M.A., Ramírez-López, E.M., 2013. Sorption mechanism of anionic dyes on pecan nut shells (*Carya illinoinensis*) using batch and continuous systems. Ind. Crops Prod. 48, 89–97. https://doi.org/10.1016/j.indcrop.2013.04.009.

Ahmadzadeh-Hakimi, K., Keshmirizadeh, E., Modarress, H., 2017. The activation of eggshell by chemical and thermal treatment for removal of acid blue 92 dye from aqueous solutions. Anal. Chem. Lett. 7, 369–382. https://doi.org/10.1080/22297928.2017.1322535.

Aljeboree, A.M., Alshirifi, A.N., Alkaim, A.F., 2017. Kinetics and equilibrium study for the adsorption of textile dyes on coconut shell activated carbon. Arab. J. Chem. 10, S3381–S3393. https://doi.org/10.1016/j.arabjc.2014.01.020.

Anbuvannan, M., Ramesh, M., Viruthagiri, G., Shanmugam, N., Kannadasan, N., 2015. Synthesis, characterization and photocatalytic activity of ZnO nanoparticles prepared by biological method. Spectrochim. Acta - Part A Mol. Biomol. Spectrosc. 143, 304–308. https://doi.org/10.1016/j.saa.2015.01.124.

Awasthi, A., Arya, A., Gupta, P., Kumar, R., Singh, J., Datta, D., 2020. Adsorption of Reactive Blue-13, an acidic dye, from aqueous solution using magnetized activated carbon. J. Chem. Eng. Data 65, 2220–2229. https://doi.org/10.1021/acs.jced.0c00081.

Awogbemi, O., Inambao, F., Onuh, E.I., 2020. Modification and characterization of chicken eggshell for possible catalytic applications. Heliyon 6,. https://doi.org/10.1016/j.heliyon.2020.e05283 e05283.

Bessashia, W., Berredjem, Y., Hattab, Z., Bououdina, M., 2020. Removal of Basic Fuchsin from water by using mussel powdered eggshell membrane as novel bioadsorbent: Equilibrium, kinetics, and thermodynamic studies. Environ. Res. 186,. https://doi.org/10.1016/j.envres.2020.109484 109484.

Binupriya, A.R., Sathishkumar, M., Jung, S.H., Song, S.H., Yun, S.I., 2009. A novel method in utilization of bokbunja seed eastes from wineries in liquid-phase sequestration of Reactive Blue 4. Int. J. Environ. Res. 3, 1–12.

Bouhadjra, K., Lemlikchi, W., Ferhati, A., Mignard, S., 2021. Enhancing removal efficiency of anionic dye (Cibacron blue) using waste potato peels powder. Sci. Rep. 11, 2090. https://doi.org/10.1038/s41598-020-79069-5.

Buthiyappan, A., Gopalan, J., Abdul Raman, A.A., 2019. Synthesis of iron oxides impregnated green adsorbent from sugarcane bagasse: Characterization and evaluation of adsorption efficiency. J. Environ. Manage. 249,. https://doi.org/10.1016/j.jenvman.2019.109323 109323.

Çelebi, H., 2019. The applicability of evaluable wastes for the adsorption of Reactive Black 5. Int. J. Environ. Sci. Technol. 16, 135–146. https://doi.org/10.1007/s13762-018-1969-3.

Chavan, R.B., 2011. Environmentally friendly dyes, Woodhead Publishing Series in Textiles. Woodhead Publishing Limited 16. https://doi.org/10.1533/9780857093974.2.515.

Chowdhury, S., Saha, T.K., 2016. Adsorption of reactive blue 4 (RB4) onto rice husk in aqueous solution. Int. J. Sci. Eng. Res. 7, 7–12.

Dos Reis, G.S., Larsson, S.H., Thyrel, M., Pham, T.N., Lima, E.C., de Oliveira, H.P., Dotto, G.L., 2021. Preparation and application of efficient biobased carbon adsorbents prepared from spruce bark residues for efficient removal of reactive dyes and colors from synthetic effluents. Coatings 11, 772. https://doi.org/10.3390/coatings11070772.

Dubinin, M.M., Radushkevich, L.V., 1947. The equation of the characteristic curve of activated charcoal. Proc. USSR Acad. Sci. 55, 327–329.

Elovich, S.Y., Larinov, O.G., 1962. Theory of adsorption from solutions of non electrolytes on solid (I) equation adsorption from solutions and the analysis of its simplest form,(II) verification of the equation of adsorption isotherm from solutions. Izv. Akad. Nauk. SSSR, Otd. Khim. Nauk. 2, 209–216.

Elsayed, M.S., Ahmed, I.A., Bader, D.M.D., Hassan, A.F., 2022. Green synthesis of nano zinc oxide/nanohydroxyapatite composites using date palm pits extract and eggshells: Adsorption and photocatalytic degradation of methylene blue. Nanomaterials 12. https://doi.org/10.3390/nano12010049.

Freundlich, H., 1906. Over the adsorption in solution. J. Phys. Chem. 57, 385–470. https://doi.org/10.1515/zpch-1907-5723.

Galan, J., Trilleras, J., Zapata, P.A., Arana, V.A., Grande-Tovar, C. D., 2021. Optimization of chitosan glutaraldehyde-crosslinked beads for reactive blue 4 anionic dye removal using a surface response methodology. Life 11, 85. https://doi.org/10.3390/life11020085.

Gupta, V.K., Nayak, A., 2012. Cadmium removal and recovery from aqueous solutions by novel adsorbents prepared from orange peel and Fe_2O_3 nanoparticles. Chem. Eng. J. 180, 81–90. https://doi.org/10.1016/j.cej.2011.11.006.

Hamdi, W.J., Habubi, N.F., 2018. Preparation of epoxy chicken eggshell composite as thermal insulation. J. Aust. Ceram. Soc. 54, 231–235. https://doi.org/10.1007/s41779-017-0145-4.

Ho, Y.S., McKay, G., 1999. Pseudo-second order model for sorption processes. Process Biochem. 34, 451–465. https://doi.org/10.1016/S0032-9592(98)00112-5.

Huang, Y., Gao, Y., Zhang, Q., Zhang, Y., Cao, J. ji, Ho, W., Lee, S. C., 2018. Biocompatible FeOOH-Carbon quantum dots nanocomposites for gaseous NO_x removal under visible light: Improved charge separation and High selectivity. J. Hazard. Mater. 354, 54–62. https://doi.org/10.1016/j.jhazmat.2018.04.071

Ibrahim, S., Fatimah, I., Ang, H.M., Wang, S., 2010a. Adsorption of anionic dyes in aqueous solution using chemically modified barley straw. Water Sci. Technol. 62, 1177–1182. https://doi.org/10.2166/wst.2010.388.

Ibrahim, S.M., Naghmash, M.A., El-Molla, S.A., 2020. Synthesis and application of nano-hematite on the removal of carcinogenic textile remazol red dye from aqueous solution. Desalin. Water Treat. 180, 370–386. https://doi.org/10.5004/dwt.2020.25063.

Ibrahim, S., Shuy, W.Z., Ang, H.-M., Wang, S., 2010b. Preparation of bioadsorbents for effective adsorption of a reactive dye in aqueous solution. ASIA-PACIFIC J. Chem. Eng. 5, 563–569. https://doi.org/10.1002/apj.

Jangkorn, S., Youngme, S., Praipipat, P., 2022. Comparative lead adsorptions in synthetic wastewater by synthesized zeolite A of recycled industrial wastes from sugar factory and power plant. Heliyon 8, e09323. https://doi.org/10.1016/j.heliyon.2022.e09323.

Katheresan, V., Kansedo, J., Lau, S.Y., 2018. Efficiency of various recent wastewater dye removal methods: a review. J. Environ. Chem. Eng. 6, 4676–4697. https://doi.org/10.1016/j.jece.2018.06.060.

Kaur, Y., Jasrotia, T., Kumar, R., Chaudhary, G.R., Chaudhary, S., 2021. Adsorptive removal of eriochrome black T (EBT) dye by using surface active low cost zinc oxide nanoparticles: a comparative overview. Chemosphere 278,. https://doi.org/10.1016/j.chemosphere.2021.130366 130366.

Kumar, M., Dosanjh, H.S., Singh, H., 2018. Magnetic zinc ferrite–chitosan bio-composite: synthesis, characterization and adsorption

behavior studies for cationic dyes in single and binary systems. J. Inorg. Organomet. Polym. Mater. 28, 880–898. https://doi.org/10.1007/s10904-017-0752-0.

Kumar, M., Dosanjh, H.S., Singh, H., 2019. Surface modification of spinel ferrite with biopolymer for adsorption of cationic and anionic dyes in single and ternary dye system. Fibers Polym. 20, 739–751. https://doi.org/10.1007/s12221-019-8462-6.

Kumar, M., Vijayakumar, G., Tamilarasan, R., 2019. Synthesis, characterization and experimental studies of nano Zn–Al–Fe3O4 blended alginate/Ca beads for the adsorption of rhodamin B. J. Polym. Environ. 27, 106–117. https://doi.org/10.1007/s10924-018-1318-0.

Lagergren, S., 1898. About the theory of so-called adsorption of soluble substances. K. Sven. Vetenskapsakademiens Handl. 24, 1–39.

Lakouraj, M.M., Mojerlou, F., Zare, E.N., 2014. Nanogel and superparamagnetic nanocomposite based on sodium alginate for sorption of heavy metal ions. Carbohydr. Polym. 106, 34–41. https://doi.org/10.1016/j.carbpol.2014.01.092.

Langmuir, I., 1918. The adsorption of gases on plane surfaces of glass, mica and platinum. J. Am. Chem. Soc. 40, 1361–1403.

Lawal, I.A., Chetty, D., Akpotu, S.O., Moodley, B., 2017. Sorption of Congo red and reactive blue on biomass and activated carbon derived from biomass modified by ionic liquid. Environ. Nanotechnol. Monit. Manag. 8, 83–91. https://doi.org/10.1016/j.enmm.2017.05.003.

Lellis, B., Fávaro-Polonio, C.Z., Pamphile, J.A., Polonio, J.C., 2019. Effects of textile dyes on health and the environment and bioremediation potential of living organisms. Biotechnol. Res. Innov. 3, 275–290. https://doi.org/10.1016/j.biori.2019.09.001.

Lulit, H., Natnael, S., Dure, M., Thriveni, T., Ramakrishna, C., Ji, W. A., 2019. Synthesis of nano-calcium oxide from waste eggshell by sol-gel method. Sustainability 11, 2–10.

Lv, T., Li, B., 2021. Preparation of novel magnetic sodium alginate-ferric(III) gel beads and their super-efficient removal of direct dyes from water. J. Polym. Environ. 29, 1576–1590. https://doi.org/10.1007/s10924-020-01977-4.

Ma, J., Hou, L., Li, P., Zhang, S., Zheng, X., 2021. Modified fruit pericarp as an effective biosorbent for removing azo dye from aqueous solution: study of adsorption properties and mechanisms. Environ. Eng. Res. 27,. https://doi.org/10.4491/eer.2020.634 200634.

Manzoor, J., Sharma, M., 2019. Impact of textile dyes on human health and environment. Impact Text. Dye. Public Heal. Environ. 162–169. https://doi.org/10.4018/978-1-7998-0311-9.ch008.

Monsef Khoshhesab, Z., Souhani, S., 2018. Adsorptive removal of reactive dyes from aqueous solutions using zinc oxide nanoparticles. J. Chinese Chem. Soc. 65, 1482–1490. https://doi.org/10.1002/jccs.201700477.

Nayeri, D., Mousavi, S.A., 2020. Dye removal from water and wastewater by nanosized metal oxides - modified activated carbon: a review on recent researches. J. Environ. Heal. Sci. Eng. 18, 1671–1689. https://doi.org/10.1007/s40201-020-00566-w.

Ngamsurach, P., Nemkhuntod, S., Chanaphan, P., Praipipat, P., 2022. Modified beads materials from recycled wastes of bagasse and bagasse fly ash with iron(III) oxide-hydroxide and zinc oxide for the removal of reactive blue 4 dye in aqueous solution. ACS Omega. https://doi.org/10.1021/acsomega.2c03250.

Ngamsurach, P., Praipipat, P., 2021. Modified alginate beads with ethanol extraction of *Cratoxylum formosum* and *Polygonum odoratum* for antibacterial activities. ACS Omega 6, 32215–32230. https://doi.org/10.1021/acsomega.1c05056.

Ngamsurach, P., Praipipat, P., 2022. Antibactrial activities against *Staphylococcus aureus* and *Escherichia coli* of extracted *Piper betle* leaf materials by disc diffusion assay and batch experiments. RSC Advances 12, 26435–26454. https://doi.org/10.1039/d2ra04611c.

Nouri, L., Hemidouche, S., Boudjemaa, A., Kaouah, F., Sadaoui, Z., Bachari, K., 2020. Elaboration and characterization of photobio-composite beads, based on titanium (IV) oxide and sodium alginate biopolymer, for basic blue 41 adsorption/photocatalytic degradation. Int. J. Biol. Macromol. 151, 66–84. https://doi.org/10.1016/j.ijbiomac.2020.02.159.

Omo-Okoro, P.N., Daso, A.P., Okonkwo, J.O., 2018. A review of the application of agricultural wastes as precursor materials for the adsorption of per- and polyfluoroalkyl substances: a focus on current approaches and methodologies. Environ. Technol. Innov. 9, 100–114. https://doi.org/10.1016/j.eti.2017.11.005.

Razali, S.Z., Aziz, M.Y., Edinur, H.A., Razali Ishak, A., 2020. Adsorption of methylene blue onto iron oxide magnetic nanoparticles coated with sugarcane bagasse. IOP Conf. Ser. Earth Environ. Sci. 596. https://doi.org/10.1088/1755-1315/596/1/012052.

Rey, C., Combes, C., Drouet, C., Grossin, D., Bertrand, G., Soulié, J., 2017. Bioactive calcium phosphate compounds: physical chemistry. Compreh. Biomater. II. https://doi.org/10.1016/B978-0-12-803581-8.10171-7.

Said, A.-E.-A.-A., Aly, A.A.M., El-Wahab, M.M.A., Soliman, S.A., El-Hafez, A.A.A., Helmey, V., Goda, M.N., 2013. Application of modified bagasse as a biosorbent for reactive dyes removal from industrial wastewater. J. Water Resour. Prot. 5, 10–17. https://doi.org/10.4236/jwarp.2013.57a003.

Shokry Hassan, H., Elkady, M.F., El-Shazly, A.H., Bamufleh, H.S., 2014. Formulation of synthesized zinc oxide nanopowder into hybrid beads for dye separation. J. Nanomater. 2014,. https://doi.org/10.1155/2014/967492 967492.

Teixeira, R.A., Lima, E.C., Benetti, A.D., Thue, P.S., Cunha, M.R., Cimirro, N.F.G.M., Sher, F., Dehghani, M.H., dos Reis, G.S., Dotto, G.L., 2021. Preparation of hybrids of wood sawdust with 3-aminopropyl-triethoxysilane. application as an adsorbent to remove Reactive Blue 4 dye from wastewater effluents. J. Taiwan Inst. Chem. Eng. 125, 141–152. https://doi.org/10.1016/j.jtice.2021.06.007.

Temkin, M.I., Pyzhev, V., 1940. Kinetics of ammonia synthesis on promoted iron catalysts. Acta Physiochim. URSS 12, 327–356.

Threepanich, A., Praipipat, P., 2021. Powdered and beaded lemon peels-doped iron (III) oxide-hydroxide materials for lead removal applications: synthesis, characterizations, and lead adsorption studies. J. Environ. Chem. Eng. 9,. https://doi.org/10.1016/j.jece.2021.106007 106007.

Threepanich, A., Praipipat, P., 2022. Efficacy study of recycling materials by lemon peels as novel lead adsorbents with comparing of material form effects and possibility of continuous flow experiment. Environ. Sci. Pollut. Res. 29, 46077–46090. https://doi.org/10.1007/s11356-022-19131-z.

Tizo, M.S., Blanco, L.A.V., Cagas, A.C.Q., Dela Cruz, B.R.B., Encoy, J.C., Gunting, J.V., Arazo, R.O., Mabayo, V.I.F., 2018. Efficiency of calcium carbonate from eggshells as an adsorbent for cadmium removal in aqueous solution. Sustain. Environ. Res. 28, 326–332. https://doi.org/10.1016/j.serj.2018.09.002.

Ullhyan, A., 2014. Adsorption of Reactive Blue-4 dye from aqueous solution onto acid activated mustard stalk: equilibrium and kinetic studies. Glob. J. Biol. Agric. Heal. Sci. 3, 98–105.

Weber, W.J., Morris, J.C., 1963. Kinetics of adsorption carbon from solution. J. Sanit. Eng. Div. 89, 31–60.